Tampere University of Technology
Department of Information Technology

Mohammad Zahidul Hasan Bhuiyan

Analyzing Code Tracking Algorithms for Galileo Open Service Signal

Master of Science Thesis

Subject Approved by Department Council
10.05.2006
Examiners: Prof. Markku Renfors
Dr. Elena-Simona Lohan

Preface

This Master of Science Thesis has been written for the Department of Information Technology at the Tampere University of Technology, Tampere, Finland. The work for this thesis has been performed at the Institute of Communications Engineering under Advanced Techniques for Mobile Positioning project, funded by the National Technology Agency of Finland (Tekes).

I would like to express my deep appreciation to my supervisors **Prof. Markku Renfors** and **Dr. Elena-Simona Lohan** for their tremendous encouragement, valuable guidance and for providing excellent research opportunities during my M.Sc. studies. I would like to thank Dr. Abdelmonaem Lakhzouri, Dr. Ridha Hamila, Yuan Yang, Saju Raj Singh, Elina Pajala and Adina Burian for their friendly support during the work. I also want to thank my Bangladeshi friends in Tampere for their great enjoyable company during the days of my M.Sc. studies. Finally, I express my gratitude to my parents for their endless love and inspiration.

This endeavor is dedicated to my fiancé **Mehjabin Sultana Dolan**.

Tampere, August 9, 2006

Mohammad Zahidul Hasan Bhuiyan

Insinöörinkatu 60 A 52
33720 Tampere
Finland
mohammad.bhuiyan@tut.fi
Tel. +358 407387898

Contents

Abstract

Tampere University of Technology
Degree Program in Information Technology, Institute of Communications Engineering
Bhuiyan, Mohammad Zahidul Hasan: Analyzing Code Tracking Algorithms for Galileo Open Service Signal
Master of Science Thesis, 74 pages
Examiners: Prof. Markku Renfors, Dr. Elena-Simona Lohan
Funding: National Technology Agency of Finland (Tekes)
August 2006

The ever-increasing public interest on location and positioning services has originated a demand for higher performance Global Navigation Satellite Systems (GNSSs). Galileo Open Service (OS) signal, part of the European contribution to future GNSS, was designed to respond to the above demand. In all GNSSs, the estimation with high accuracy of the Line-Of-Sight (LOS) delay is a prerequisite. The Delay Lock Loops (DLLs) and their enhanced variants (i.e., feed-back code tracking loops) are the structures of choice for the commercial GNSS receivers, but their performance in severe multipath scenarios is still rather limited. In addition, the new satellite positioning system proposals specify the use of a new modulation, the Binary Offset Carrier (BOC) modulation, which triggers a new challenge in the code tracking stage. Therefore, in order to meet this emerging challenge and to improve the accuracy of the delay estimation in severe multipath scenarios, this thesis analyzes feed-back as well as feed-forward code tracking algorithms and proposes a novel algorithm, namely Peak Tracking (PT), which is a combination of both feed-back and feed-forward structures and utilizes the advantages inherent in these structures.

In this thesis, the code tracking algorithms are studied and analyzed for Sine BOC (Sin-BOC) modulated Galileo OS signal for various multipath profiles in Rayleigh fading channel model. The performance of the analyzed algorithms are measured in terms of various well-known criteria such as Root-Mean-Square-Error (RMSE), Mean-Time-to-Lose Lock (MTLL), delay error variance and Multipath Error Envelopes (MEEs). The simulation results show that the proposed PT algorithm outperforms all other analyzed algorithms in

various multipath profiles in good Carrier-to-Noise-Ratios (CNRs). The simulation results are compared with the theoretical Cramer-Rao Bound (CRB) and the comparison shows that the delay error variance for PT algorithm approaches the theoretical limit with the increase in CNR. Therefore, the proposed algorithm can be considered as an excellent candidate for implementation in future Galileo receivers, especially when tracking accuracy is a concern.

List of Abbreviations

ACF	AutoCorrelation Function
AWGN	Additive White Gaussian Noise
AltBOC	Alternative Binary Offset Carrier
BPF	Band Pass Filter
BW	BandWidth
BOC	Binary Offset Carrier
BPSK	Binary Phase Shift Keying
C/A	Coarse/Acquisition
CASM	Coherent Adaptive Subcarrier Modulation
CDMA	Code Division Multiple Access
CNR	Carrier-to-Noise-Ratio
CosBOC	Cosine Binary Offset Carrier
COSPAS	COsmicheskaya Sistyema Poiska Avariynich Sudov
CRB	Cramer-Rao Bound
CS	Commercial Service
Diff2	Differential Order 2
DLL	Delay Lock Loop
DoD	Department of Defense
DoT	Department of Transportation
DS	Direct Sequence
DS-CDMA	Direct Sequence - Code Division Multiple Access
DSSS	Direct Sequence Spread Spectrum
EML	Early Minus Late
EU	European Union
ESA	European Space Agency
FDMA	Frequency Division Multiple Access
FH	Frequency Hopping
FH-CDMA	Frequency Hopping - Code Division Multiple Access
GJU	Galileo Joint Undertaking

GLONASS	GLobal Orbiting NAvigation Satellite System
GNSS	Global Navigation Satellite System
GPS	Global Positioning System
HRC	High Resolution Correlator
I&D	Integrate and Dump
LOS	Line-Of-Sight
MAI	Multiple Access Interface
MBOC	Multiplexed Binary Offset Carrier
MC	Multi-Carrier
MCRLB	Modified Cramer-Rao Lower Bound
MEDLL	Multipath Estimating Delay Lock Loop
MEE	Multipath Error Envelope
MEO	Medium Earth Orbit
MF	Matched Filter
MGD	Multiple Gate Delay
MOT	Advanced Techniques for Mobile Positioning
MTLL	Mean-Time-to-Lose Lock
NCO	Numerically Controlled Oscillator
NLOS	Non-Line-Of-Sight
NRZ	Non-Return to Zero
OS	Open Service
P	Precision
PAC	Pulse Aperture Correlator
PDA	Personal Digital Assistant
PDF	Probability Density Function
PPS	Precise Positioning Service
PRN	Pseudo-Random Noise
PRS	Public Regulated Service
PSD	Power Spectral Density
PT	Peak Tracking
RF	Radio Frequency
RMSE	Root Mean Square Error
SAR	Search And Rescue service
SARSAT	Search And Rescue Satellite-Aided Tracking
SD	Slope Differential
SinBOC	Sine Binary Offset Carrier

SoL	Safety of Life service
SPS	Standard Positioning Service
TDMA	Time Division Multiple Access
TH	Time Hopping
TH-CDMA	Time Hopping - Code Division Multiple Access
ToA	Time-of-Arrival
UMTS	Universal Mobile Telecommunication System
US	United States
WLAN	Wireless Local Area Network

List of Symbols

α	Fading amplitude
α_m	Complex channel coefficient of the m-th path
γ	Decision threshold
Ω	Average power of fading amplitudes
λ	Wavelength of the signal
μ	Mean of a Gaussian random variable
σ^2	Variance of a Gaussian random variable
η	AWGN noise
τ	Delay error
τ_{acq}	Coarse estimate of the code delay at code acquisition stage
$\hat{\tau}$	Estimated delay error
τ_Δ	Distance between the direct LOS component and the successive path
τ_d	Dwell time
τ_e	Excess time delay
τ_m	Delay of the m^{th} component signal of a multipath signal
$\hat{\tau}_{LOS}$	Estimated delay of LOS path
$\epsilon(\cdot)$	Spreading operation
$\epsilon^{-1}(\cdot)$	Despreading operation
δ	Normalized delay error; $(\tau - \hat{\tau})/T_c$
Δ	Early-late chip spacing
Δ_{inc}	Channel delay increment
Δ_{NEML}	Early-late chip spacing for narrow EML
Δ_{WEML}	Early-late chip spacing for wide EML
$\Delta\Delta$	Double delta correlator
$(\Delta f)_c$	Coherence bandwidth
$(\Delta f)_{ds}$	Doppler spread
$(\Delta t)_c$	Coherence time
θ_m	Phase of the m^{th} component signal of a multipath signal
a_i	Weight based on peak height for i^{th} competitive peak

A_m	Amplitude of the m^{th} component signal of a multipath signal
A	Average first path power
ACF_{Peak}	Peak in ACF domain
ACF_{Thresh}	Threshold chosen for ACF domain
b_i	Weight based on peak position for i^{th} competitive peak
b_n	Data bit
B_W	Bandwidth
c	Speed of light; $c = 3 * 10^8$ m/s
c_i	Weight based on previous estimation for i^{th} competitive peak
C_{Peak}	Competitive Peak
d	Distance between the source and receiver
d_i	Decision variable for i^{th} competitive peak; $d_i = a_i b_i c_i$
$Diff2_{Peak}$	Peak in Diff2 domain
$Diff2_{Thresh}$	Threshold chosen for Diff2 domain
E_b	Bit energy
f	Frequency
f_c	Carrier frequency
f_D	Doppler shift
f_{chip}	Chip rate
f_{sc}	Subcarrier frequency
g	Gaussian random variable
K	Rician factor
l_{max}	Maximum value in Diff2 domain
L	Path loss
$\hat{L}$	Cardinality of the set C_{Peak}; $\hat{L} = \|C_{Peak}\|$
M	Number of multipaths
m	Nakagami-m fading parameter
n^2	Rician factor; $(n^2 = K)$
N_{BOC}	BOC modulation order
N_C	Coherent integration length in code epochs (or ms)
N_{NC}	Non-coherent integration length in blocks
N_S	Oversampling factor
N_{Thresh}	Noise threshold
P_d	Detection probability
P_{fa}	False alarm probability
R	Bit rate

S_F	Spreading factor or code epoch length in chips
S_n	Narrowband signal before modulation
S_w	Wideband signal after modulation
s_{SinBOC}	SinBOC subcarrier
T_c	Chip period; $1/f_{chip}$
T_m	Delay spread
v_m	Mobile speed of the receiver
v_s	Speed of the satellite
W_{ACF}	Weight factor for ACF
W_D	Weight factor for Diff2
x_{data}	Data sequence after spreading
x_{PRN}	PRN code sequence
x_{SinBOC}	Data sequence after spreading and SinBOC modulation

Chapter 1

Introduction

Today, with the glorious advance in satellite navigation and positioning technology, it is possible to pinpoint the exact location of any user anywhere on the surface of the globe at any time of day or night. Since its launch in the 1970s, the United States (US) Global Positioning System (GPS), has become the universal satellite navigation system and reached full operational capability in 1990s [1]. This has created a monopoly, resulting in technical, political, strategic and economic dependence for millions of users. In recent years, the rapid improvement and lowered price of computing power have allowed the integration of GPS chips into small autonomous devices such as hand-held GPS receivers, Personal Digital Assistants (PDAs), and cellular phones, increasing the speed of its consumption by the general public. In order to capitalize on this massive rising demand, and to cope with civil and military expectations in terms of performance, several projects were launched to give birth to a second generation of Global Navigation Satellite Systems (GNSSs) in the 1990s [2]. This led to two major GNSS decisions: the modernization of the current US GPS, known as GPS I, and the independent European effort to create its own GNSS, known as Galileo. These two systems are now being finalized and are expected to be available to the public by the end of the decade. It is anticipated that once the new European satellite navigation system Galileo is operational, the vast majority of all user receivers sold will be both GPS and Galileo capable. The benefits of receiving signals from both constellations include improved accuracy, reliability, and availability.

1.1 Background and Motivations

The early success encountered by GPS I combined with a substantial potential for growth in positioning and timing applications in the civilian market are the major reasons for a world-wide modernization effort. In the 1990s, the US Department of Defense (DoD) and Department of Transportation (DoT) started a GPS modernization process, called GPS

II and GPS III [2]. The European Union (EU) and the European Space Agency (ESA) decided to launch their own GNSS, i.e., Galileo [3]. Finally, Russia decided to re-activate its GLobal Orbiting NAvigation Satellite System (GLONASS) program [4].

Among the signals proposed for Galileo system, the Galileo Open Service (OS) signal, transmitted in L1F band with center frequency 1575.42 MHz, is of particular interest for several reasons. Firstly, it is designed for mass-market users. A mass-market signal means that every Galileo user will have access to this signal, and it should be the target signal for most of the autonomous and leisure-oriented applications such as mobile phones and PDAs, implying a very large potential market. Consequently, it is Galileo's direct counterpart to the current GPS I civil signal. In order to appeal to a wide range of civilian users and personal navigation in particular, the signal design should be such that it does not require an immense amount of processing power for tracking while still providing optimal positioning capabilities in degraded signal environments. The significance of these factors has spurred much research into the receiver design adaptations necessary to take full advantage of this signal.

Secondly, it is important to identify and assess any improvement for mass-market users brought by the use of the Galileo OS signal compared to what is currently available to them through the GPS Coarse/Acquisition (C/A) signal.

Finally, the Galileo OS signal uses new modulation that is also used by other GPS II and Galileo signals [5]. Therefore, the knowledge gained from research and analysis with this particular signal can be transposed for improving other signal profiles.

The innovation brought by the use of Binary Offset Carrier (BOC) modulation for the Galileo OS signal is of central interest for tracking performance as it leads to substantial improvement in tracking. BOC modulation was chosen as the chief candidate for several future navigation signals for various purposes. Its split spectrum property allows the reduction of spectral overlapping with other GPS signals and, thus, lessens the potential for interference with the GPS legacy signals that have their energy around the carrier frequency. Another implication for non-overlapping signals is the possibility for the US military to jam civil signals without losing the military signals. Of the several BOC families available, a relevant choice of this modulation can drastically limit inter- and intra-system interference [6, 7]. Moreover, BOC modulation has very interesting tacking property of outperforming an equivalent Binary Phase Shift Keying (BPSK) modulation in terms of resistance to thermal noise, narrow-band interference rejection and multipath mitigation [6].

However, despite these advantages, there are some challenges with the use of BOC modulation. BOC signal tracking shows potential false lock points [6, 8]. This stems from the

BOC AutoCorrelation Function (ACF), which is characterized by multiple side peaks with non-negligible magnitudes. Undergoing a false lock produces biased measurements and, therefore, an unacceptable result for a system that aims to provide an accurate navigation solution. Consequently, solutions have to be found to minimize this bias threat in order to be able to use BOC signals in a GNSS. Many studies have been published on the tracking ambiguity of BOC signals, for example, in [9], [10] and in [11]. Most of these methods try to resolve the tracking ambiguity problem in the same fashion for all BOC families. In reality, there exist different BOC families with characteristics defined by the spectral separation and width of the side lobes. Although the families may be derived in a similar way, a single resolution to the ambiguous tracking problem may not be optimal for all signals. Therefore, an innovative tracking technique dedicated to a certain BOC family might provide a more effective solution in the same way that some tracking techniques are optimal for BPSK modulations but not for other types of modulations. This was the prior motivation of this thesis to focus on Sine BOC(1,1), denoted here by SinBOC(1,1), which has already been selected as the modulation technique for the Galileo OS signal.

1.2 Thesis Objectives

This thesis is part of the Advanced Techniques for Mobile Positioning (MOT) project which has been carried out at Tampere University of Technology. The one main objective of the project was to develop and analyze the implementation possibilities of various code tracking architectures for the modernized GPS and Galileo systems.

The aim of this thesis is to investigate the performance of different code tracking algorithms for Galileo OS signal which incorporates the new innovation brought by BOC modulation. Since the signal of interest is the Galileo OS, the solution presented in this thesis will be relevant to this particular signal, even if it may not work for all BOC families. To find an effective solution, a new code tracking algorithm was developed.

1.3 Thesis Contributions

The major contributions of the thesis are enumerated below:

- A detail analysis of the few significant code tracking algorithms in terms of Root Mean Square Error (RMSE), Mean-Time-to-Lose Lock (MTLL), delay error variance and semi-analytical Multipath Error Envelopes (MEEs),
- A study of the tolerance of traditional feed-back code tracking algorithms in the presence of initial delay error fed from the code acquisition stage,

- The development and test of a new code tracking algorithm, namely Peak Tracking (PT), for Galileo OS signal.

1.4 Thesis Outline

In order to provide a comprehensive view of the research realized by the thesis, this document has been structured in the following way:

Chapter 1 provides a brief illustration of the scope of the thesis including its motivations, objectives and contributions followed by the overall thesis outline.

Chapter 2 familiarizes the reader with the concepts necessary to understand the basics of satellite based positioning. It also provides an introduction to GPS and Galileo systems followed by a brief presentation on Galileo signal characteristics. Finally, BOC modulation description is given.

Chapter 3 discusses the fundamentals of spread spectrum techniques while the main focus is always restricted to Direct Sequence - Code Division Multiple Access (DS-CDMA) scheme since DS-CDMA is the most widely used method in satellite systems and both GPS and Galileo systems employ DS-CDMA method in satellite communications.

Chapter 4 covers the propagation aspects and the fading channel characteristics for wireless systems. It also includes a short overview of the fading channel models with different fading types and distributions. Finally, the meaning of Carrier-to-Noise-Ratio (CNR) is explained in the context of the thesis.

Chapter 5 presents an in-depth discussion on code synchronization mechanism in DS-CDMA systems. It firstly describes the code acquisition task, which consists of a search stage and a detection stage, followed by code tracking architecture with emphasis on Delay Lock Loop (DLL).

Chapter 6 is a thorough study of several code tracking algorithms for both feed-back and feed-forward structures. The few significant code tracking algorithms are briefly analyzed in this chapter with substantial references given for detailed explanations.

Chapter 7 introduces a novel innovative code tracking algorithm for SinBOC(1,1) modulated signal which is referred as Peak Tracking. This new technique is first described in great theoretical detail. Its critical parameters and thresholds are explained in detail with graphical presentations whenever necessary. Finally, the procedure of PT algorithm is presented with one illustrative example.

In **Chapter 8**, the performance of different code tracking algorithms along with the proposed PT algorithm is presented in terms of RMSE, MTLL, delay error variance and

semi-analytical MEEs. Simulation results are provided for various multipath profiles in Rayleigh fading channel model in order to realize the performance of the discussed code tracking algorithms. Results obtained from the simulations are then compared with the theoretical Cramer-Rao Bound (CRB). At last, the performance of feed-back code tracking algorithms and the proposed PT algorithm is shown in terms of MEEs.

Finally, **Chapter 9** draws conclusions from this research and points out future research directions.

Chapter 2

Satellite-Based Positioning

Mobile positioning has gained increasing attention during the past few years. A number of new positioning techniques have evolved over the years. They can be classified in two major categories: satellite-based and cellular-based positioning technology. The scope of the thesis is limited to satellite-based positioning technology, therefore, a brief introduction to satellite-based navigation systems, e.g., Navstar GPS and Galileo, is provided in this chapter. Also, later in this chapter, the Galileo signal structure and the new modulation technique, i.e., BOC, are presented based on the current standardization documents.

2.1 Satellite-Based Positioning Technique

Since immemorial times, people have looked to the heavens to find their way. Today, satellite navigation is continuing this tradition, while offering an accuracy far beyond the early days when positioning was done by simply observing the sun and the stars. This technology, which has been developed over the last thirty years or so, essentially for military purposes, enables anyone with a receiver capable of picking up signals emitted by a constellation of satellites to instantly determine their position in time and space very accurately.

The operating principle is simple: both GPS and Galileo systems use the Time-of-Arrival (ToA) measurements in order to determine the accurate location of the receiver. The position of the user is determined by estimating the propagation time it takes for a signal to arrive at the receiver from the transmitter (i.e., satellite). This can be done by finding the timing of the received signal (i.e., receiving moment), which is usually performed via a synchronization process in spread spectrum systems which will be described later in Chapter 5. Since the transmission time can be measured from the received data, the propagation delay can be further calculated as the difference between the transmission and the receiving moments. The propagation time is then multiplied with the speed of the

signal (i.e., the speed of light), and hence, the distance between the transmitter and the receiver is obtained. Naturally, the distance defined via one satellite leads to a circle, on which the receiver should lie, since the direction of the signal is not known [12]. When the signal is transmitted from several satellites with known locations, simultaneously, and the distances between the receiver and each satellite can be estimated, the receiver can define its location with high accuracy. In practice, at least 4 satellites (i.e., 3 for 3 dimensional space coordinates x, y, z and the remaining for time dimension t) are needed, in order to be able to calculate the position and also the speed of the receiver has to be known. In Figure 2.1, the signal arrives from three different satellites. The crossing point of the three measured distances is the precise location of the user. [1]

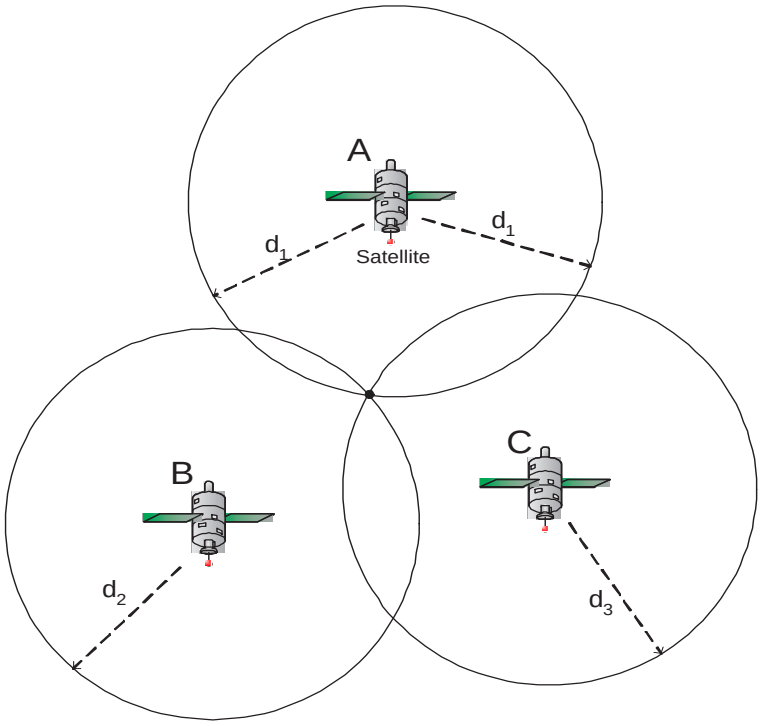

Figure 2.1: Position determination using distance d measurements from three sources [1]

Usually, it is assumed that the signal is propagating along a direct line (Line-Of-Sight, LOS) path between the satellite and the receiver. However, positioning needs to be carried out in all the environments covered by the wireless communication services, including the most constraining areas such as dense urban areas and obstructed indoor environments [1]. The signal transmitted from the satellites experiences severe attenuation while penetrating all the construction materials making the visibility with the sky quite rare, besides that the indoor propagation of satellite signals are not well understood yet [13].

2.2 Global Positioning System

The Navstar GPS is a constellation of orbiting satellites that provides navigation data to military and civilian users all over the world. GPS is a space-based radio-positioning and time transfer system. Presently, GPS is fully operational and meets the criteria established in the 1960s for an optimum positioning system. The system provides accurate, continuous, worldwide, three-dimensional position and velocity information to users with the appropriate receiving equipment. GPS can provide service to an unlimited number of users since the user receivers operate passively (i.e., receive only). [1]

The satellite constellation in GPS consists of 24 satellites arranged in 6 orbital planes with 4 satellites per plane. Since the ToA measurement is based on the timing information as explained in the previous section, possible clock offsets between the satellite and receiver equipment might cause errors on the positioning accuracy. Therefore, a fourth satellite is used to help with the clock time synchronization. Thus, four measurements are required to determine user latitude, longitude, height and receiver clock offset from receiver system time. [1]

GPS provides two services: Standard Positioning Service (SPS) and Precise Positioning Service (PPS). SPS is designed for the civil community, whereas PPS is available only for military use. SPS provides positioning with an accuracy of at least 100 meters in horizontal direction, whereas PPS provides positioning with higher degree of precision (at least 22 meters in horizontal plane). [1]

GPS signals use a Direct Sequence Spread Spectrum (DSSS) technique, and are based on Code Division Multiple Access (CDMA) principles to distinguish signals coming from different satellites [14, 15]. Spread spectrum and CDMA techniques are elaborately discussed in Chapter 3. The basic GPS signals are transmitted into two frequency bands: L1 centered at 1575.42 MHz, and L2 centered at 1227.6 MHz, among which L1 is the primary frequency band. The carrier signals are modulated by the spreading codes using BPSK modulation. Each satellite uses the same frequencies, but the signals are separated with specific spreading codes in order to avoid interference and to be able to detect the desired signal. In GPS, there are two basic code types: a short C/A code with 1 ms period, and a long Precision (P) code. P code is further encrypted with so-called Y code, which is available only for PPS users. The code length for the GPS C/A signal is 1023 chips. [1]

The modernization of the GPS system became obvious when the design of a new signal with better performance and flexibility was started. The modernized GPS includes a new frequency band L5 (1176.45) and new signals: a new military M signal, a new civil L2C signal and a new wider bandwidth civil L5 signal. The M signal will operate on both

L1 and L2 frequency bands, the L2C signal on the L2 frequency band, and respectively, the L5 signal will operate on the L5 frequency band. It has been decided that the new modulation type for the new M signal will be BOC modulation. A brief overview of BOC modulation is presented in section 2.5. [16]

2.3 Galileo System

Galileo will be Europe's own global navigation satellite system, providing a highly accurate and guaranteed positioning service under civilian control. It will be interoperable with the two other systems: the US GPS and Russia's GLONASS. Galileo will deliver real-time positioning services with unrivaled accuracy and integrity.

The fully deployed Galileo system consists of 30 satellites (27 operational+3 active spares), positioned in three circular Medium Earth Orbit (MEO) planes at 23,222 km altitude above the Earth, and at an inclination of the orbital planes of 56 degrees with reference to the equatorial plane. Once this is achieved, the Galileo navigation signals will provide good coverage even at latitudes up to 75 degrees north, which corresponds to the North Cape and beyond. The basic idea is that at any time four satellites are located above the horizon for all points of the Earth. Galileo system is planned to be operational around 2008-2010. [17]

Galileo will provide different navigation services [17, 18] of the following types:

- The OS results from a combination of open signals, free of user charge, providing position and timing performances competitive with other GNSSs.
- The Safety of Life service (SoL) improves the OS performances providing timely warnings to the users when it fails to meet certain margins of accuracy.
- The Commercial Service (CS) provides access to two additional signals, to allow for a higher data rate throughput and to enable users to improve accuracy. This service also provides a limited broadcasting capacity for messages from service centers to users.
- The Public Regulated Service (PRS) provides position and timing to specific users requiring a high continuity of service, with controlled access. Two PRS navigation signals with encrypted ranging codes and data will be available.
- The Search And Rescue service (SAR) broadcasts globally the alert messages received from distress emitting beacons. It will contribute to enhance the performance of the international COSPAS-SARSAT (COsmicheskaya Sistyema Poiska Avariynich Sudov - Search And Rescue Satellite-Aided Tracking) search and rescue system [19].

Galileo offers a number of advantages over GPS [20]:

- Galileo has been designed and developed as a non-military application, while incorporating all the necessary protective security features. Unlike GPS, which was essentially designed for military use, Galileo therefore provides, for some of the services offered, a very high level of continuity required by modern business, in particular with regard to contractual responsibility.
- It is based on the same technology as GPS and provides a similar and possibly higher degree of precision, thanks to the structure of the constellation of satellites and the ground-based control and management systems planned.
- Galileo is more reliable as it includes a signal 'integrity message' informing the user immediately of any errors. In addition, unlike GPS, it will be possible to receive Galileo signals in towns and in regions located in extreme latitudes.
- It represents a real public service and, as such, guarantees continuity of service provision for specific applications. GPS signals, on the other hand, in recent years have on several occasions become unavailable on a planned or unplanned basis, sometimes without prior warning.

Moreover, Galileo also complements GPS as [20]:

- Using both infrastructures in a coordinated fashion (double sourcing) offers real advantages in terms of precision and in terms of security, should one of the two systems become unavailable.
- The existence of two independent systems is of benefit to all users since they will be able to use the same receiver to receive both GPS and Galileo signals.

2.4 Galileo Signal Characteristics

Figure 2.2 shows the the general view of Galileo spectrum, which consists of 4 frequency bands: E5a, E5b, E6 and E2-L1-E1. Different frequencies will be assigned to the Galileo system depending on the service type. Frequency bands are divided into lower L-band (corresponding to E5a and E5b frequency bands with carrier frequencies, $f_c = 1176.45$ MHz at E5a and $f_c = 1207.14$ MHz at E5b), middle L-band (i.e., E6 frequency band with $f_c = 1278.75$ MHz) and upper L-bands (E2-L1-E1 band with $f_c = 1575.42$ MHz) [5]. As it can be noticed, both GPS and Galileo use certain identical carrier frequencies. This guarantees the ability to attain interoperability between the two systems [18]. OS

is planned to operate on the E5a, E5b and E2-L1-E1 carriers, SAR on the E5a, E5b and E2-L1-E1 carriers, CS on the E5b and E6 carriers, and PRS on the E6 and E2-L1-E1 carriers [5].

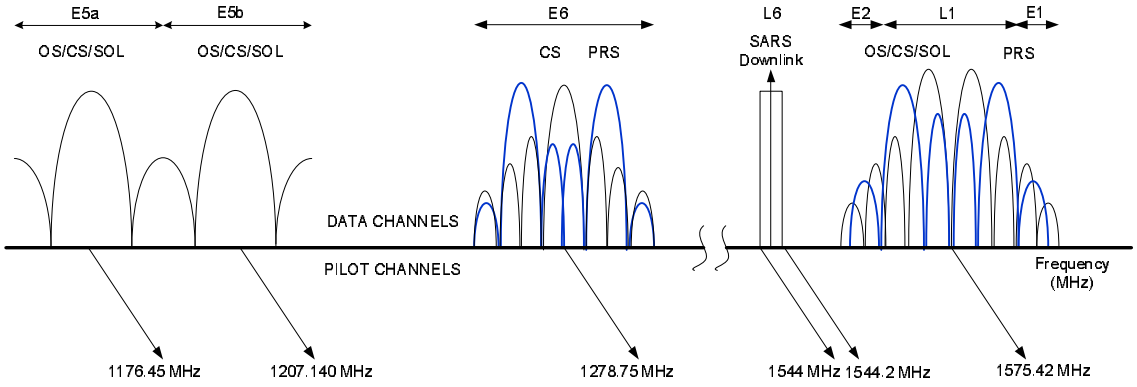

Figure 2.2: Galileo signal in space [5]

A summary of Galileo signal specifications, based on current standards [17], are shown in Table 2.1. Galileo satellite transmits six different navigation signals: L1F, L1P, E6C, E6P, E5A and E5B signals. As can be seen in Table 2.1, among these signals, L1F (open access signal) and L1P (restricted access signal) operate on the L1 Radio Frequency (RF) band, E6C (CS-signal) and E6P (PRS-signal) on the E6 band, and respectively, E5A and E5B signals are transmitted using the E5a and E5b frequency bands. Table 2.1 shows also the BandWidths (BWs), the modulation types (i.e., how the carrier frequency is modulated by the information signal), the chip rates, the multiplexing schemes, the possible availability of pilot signals, the data symbol rates and the code length for each Galileo signal as specified in Galileo Joint Undertaking (GJU) documents as from April'2006.

The most important characteristics of the Galileo signals, in comparison with the GPS signals, are the different modulation types and code lengths. SinBOC(1,1) is selected as the modulation type for the L1F OS signal, and Cosine BOC(15,2.5), denoted here as CosBOC(15,2.5), for the L1P PRS signals. The code length for the OS signal is 4092 chips, which is four times higher than the GPS C/A code length of 1023 chips. For the E5 signals, the code length is decided to be as high as 10230 chips. The multiplexing scheme here means the modulation type by which two signals are combined. For the E5 signals, the multiplexing scheme is Alternative BOC(15,10), denoted here as AltBOC(15,10), and for the L1 signals, it is Coherent Adaptive Subcarrier Modulation (CASM). [17]

A recent joint design activity of GPS-Galileo working group on interoperability and compatibility has recommended an optimized Multiplexed Binary Offset Carrier (MBOC) spreading modulation [21]. The MBOC(6,1,1/11) Power Spectral Density (PSD) is a mixture of BOC(1,1) spectrum and BOC(6,1) spectrum, that would be used by Galileo for its

Table 2.1: Galileo signal structures. N/A = Not Applicable, sps = symbols per second [5, 17, 18]

Galileo bands	RF	BW rate [MHz]	Modulation type	Chip rate [MHz]	Multiplex. scheme	Pilot availab.	Data symb. rate [sps]	Code length [chips]
L1F (OS/ CS/SoL)	L1	$40 \times 1.023 = 40.92$	SinBOC (1,1)	1.023	CASM	Yes	250	4092
L1P (PRS)	L1	40.92	CosBOC (15,2.5)	2.5575		N/A	N/A	N/A
E6C (CS)	E6	40.92	BPSK (5)	5.115	N/A	Yes	1000	N/A
E6P (PRS)	E6	40.92	CosBOC (10,5)	5.115		N/A	250	N/A
E5a (OS/ CS/PRS))	E5	$90 \times 1.023 = 90.07$	BPSK (10)	10.23	AltBOC (15,10)	Yes	50	10230
E5b (OS/ CS/PRS)	E5	90.07	BPSK (10)	10.23		Yes	250	10230

OS signal at L1 frequency, and also by GPS for its modernized L1C (i.e., L1 Civil) signal [22]. The construction and various performance characteristics of MBOC are described in [22].

Galileo L1F, which is an OS signal, free of charge, and available to any user possessing a suitable receiver, is the focus of the thesis. The modulation chosen for L1F signal (i.e., SinBOC(1,1)) is illustrated in the next section.

2.5 BOC Modulation

A new modulation type, namely the BOC modulation, has been introduced by Betz for the new military GPS system [23]. Since then, several variants have been developed: SinBOC [23], CosBOC [23] and AltBOC [5]. Later on, in June'2005, the negotiators for Galileo system architecture proposed that the modulation technique for the OS signals would be SinBOC(1,1), which uses a 1.023 MHz square subcarrier modulated by a spreading code with a chip rate of 1.023 MHz.

A BOC signal is obtained through the product of a Non-Return to Zero (NRZ) spreading code with a synchronized square wave subcarrier. This square wave can either be sine or cosine phased, which leads to different signal characteristics. They are referred to as SinBOC and CosBOC, respectively [18]. In the navigation community, the typical notation of a BOC-modulated signal is BOC(f_{sc}, f_{chip}), where f_{sc} is the subcarrier frequency in MHz and f_{chip} is the chip rate in MHz [23]. Alternatively, BOC(n, m) notation is also used,

where n and m are two indices computed from f_{sc} and f_{chip}, respectively, with respect to a reference of 1.023 MHz frequency: $n = \frac{f_{sc}}{1.023MHz}$ and $m = \frac{f_{chip}}{1.023MHz}$ with n and m being constrained to:

- positive,
- $n \geq m$, and
- ratio $N_{BOC} = 2\ \frac{n}{m} = 2\ \frac{f_{sc}}{f_{chip}}$ being a positive integer.

N_{BOC} is also called BOC modulation order. However, $N_{BOC} = 2$ represents, e.g., BOC(1,1) and BOC(2,2). Similarly, $N_{BOC} = 12$ represents, e.g., BOC(15,2.5). A special case of BOC modulation is the BPSK modulation with N_{BOC}=1. [23]

The SinBOC(1,1) modulation is part of the SinBOC(n,n) family, where the length of one subcarrier period equals one Pseudo-Random Noise (PRN) chip duration. In order to give a high-level idea of its impact on signal tracking, a few details are given herein. SinBOC(n,n) modulation splits the usual BPSK(n) spectrum into two symmetric side lobes centered at $\pm f_{sc}$ MHz around the carrier frequency. This allows a wider spectral occupancy. The SinBOC(n,n) PSD envelope is given by [23]:

$$G_{SinBOC(1,1)}(f) = f_{chip}\left(\frac{sin\left(\frac{\pi f}{2f_{chip}}\right)sin\left(\frac{\pi f}{f_{chip}}\right)}{\pi f cos\left(\frac{\pi f}{2f_{chip}}\right)}\right)^2 \tag{2.1}$$

The SinBOC(1,1) PSD envelope is shown in Figure 2.3 along with the BPSK(1) PSD envelope that represents the GPS C/A code modulation. The SinBOC(1,1) PSD has its side lobes on the zeros of the GPS C/A code PSD. As a consequence, it is well suited to have good spectral separation properties from C/A signal. This is important to avoid inter-system interference [24]. The SinBOC subcarrier is defined according to the original definition in [23]:

$$s_{SinBOC}(t) = sign\left(sin\left(\frac{N_{BOC}\pi t}{T_c}\right)\right), \tag{2.2}$$

where $sign(\cdot)$ is the signum operator and T_c is the chip period ($T_c = 1/f_{chip}$). The PRN code sequence can be defined as:

$$x_{PRN,n}(t) = \sum_{k=1}^{S_F} c_{k,n}p(t - kT_c - nT_cS_F), \tag{2.3}$$

where k is the index, n is the data symbol index, and $p(\cdot)$ is the rectangular pulse shape. After spreading, the data sequence can be expressed as:

$$x_{data}(t) = \sum_{n=-\infty}^{\infty} \sqrt{E_b}b_n x_{PRN,n}(t), \tag{2.4}$$

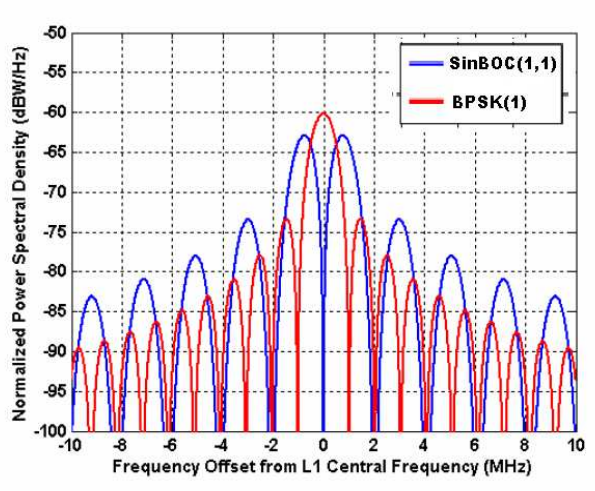

Figure 2.3: SinBOC(1,1) and BPSK(1) normalized power spectral densities

where b_n is the data bit (for the pilot channels, b_n equals to 1 for all values of n), and E_b is the bit energy. The data sequence after spreading and BOC modulation is:

$$x_{SinBOC}(t) = x_{data}(t) \otimes s_{SinBOC}(t), \tag{2.5}$$

where $\otimes$ represents the convolution operation. An equivalent model for BOC modulation is presented in [25, 26]. Based on [25, 26], the transmitted SinBOC modulated data sequence can be expressed as:

$$x_{SinBOC}(t) = \sum_{n=-\infty}^{\infty} \sum_{k=1}^{S_F} \sum_{i=0}^{N_{BOC}-1} \sqrt{E_b}(-1)^i b_n (-1)^{kN_{BOC}} c_{k,n} p(t - kT_c - nT_c S_F - i\frac{T_c}{N_{BOC}}) \tag{2.6}$$

2.5.1 Advantages of BOC Modulation

BOC modulation provides a simple and effective way of moving the signal energy away from band center, offering a high degree of spectral separation from conventional phase shift keyed signals whose energy is concentrated near band center. The resulting split spectrum signal effectively enables frequency sharing, while providing attributes that include simple implementation, good spectral efficiency, high accuracy, and enhanced multipath resolution. [23]

2.5.2 Challenges of BOC Modulation

The envelope of the ACF of a BOC modulated signal contains multiple peaks that have significant magnitudes as compared to the magnitude of the central peak. In case of SinBOC(1,1) modulation, the two side peaks of the correlation function have magnitudes

that are nearly half of the magnitude of the central peak, as is evident from Figure 2.4. This means that a signal tracker can lock onto the wrong peak, thus producing a tracking error. Figure 2.4 depicts the fact that as compared to BPSK(1) signal, the envelope of a SinBOC(1,1) modulated signal possesses two additional peaks at about $\pm$ 0.5 chips apart from the maximum peak of ACF. This is the case for single path channel profile. The

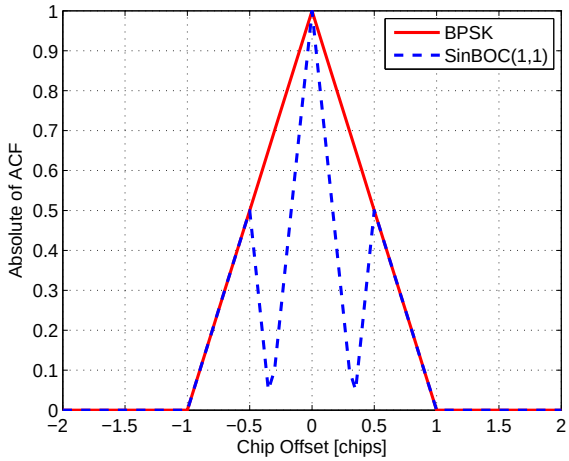

Figure 2.4: Absolute of ACF for SinBOC(1,1) and BPSK(1)

situation could be far worse in multipath fading channel model and it can make the correct delay estimation more challenging. Therefore, this is really an open issue to overcome the false tracking to the wrong peak, especially in multipath fading channel model. Hence, the main research focus of the thesis is to cope with the challenge of tracking ambiguity as much as possible in case of multipath fading channel model. The details about code tracking will be discussed in Chapter 5.

Chapter 3

Spread Spectrum Techniques

Spread spectrum communications, with their inherent interference attenuation capability, have over the years become increasingly popular techniques for use in many different systems. Now-a-days, spread spectrum techniques are used in many digital communication systems, such as 3^{rd} generation mobile communications (i.e., Universal Mobile Telecommunication System (UMTS)), GPS, Galileo, Wireless Local Area Network (WLAN) and alike. A definition of spread spectrum that adequately reflects the characteristics of this technique is: *Spread spectrum is a means of transmission in which the signal occupies a bandwidth in excess of the minimum necessary to send the information; the band spread is accomplished by means of a code which is independent of the data, and a synchronized reception with the code at that receiver is used for despreading and subsequent data recovery* [27]. One main advantage of this technique is that several users can utilize the same frequency band simultaneously [28]. Fundamentals of spread spectrum techniques are discussed in this chapter.

3.1 Multiple Access

Multiple access refers to the sharing of a common resource to allow simultaneous communications by multiple users in a single transmission medium. Due to the fact that the available bandwidth is limited to a certain amount, the main question usually is how to share the transmission band effectively between multiple users [29]. In radio communications, the interface between the user and the network is a radio interface, and the shared common resource is therefore the RF spectrum. The RF spectrum can, however, be shared by employing different strategies, so there are different techniques of providing multiple access as shown in Figure 3.1.

For radio systems, there are two resources: time and frequency. Division by time, so that each pair of communicators is allocated all (or at least a large part) of the spectrum

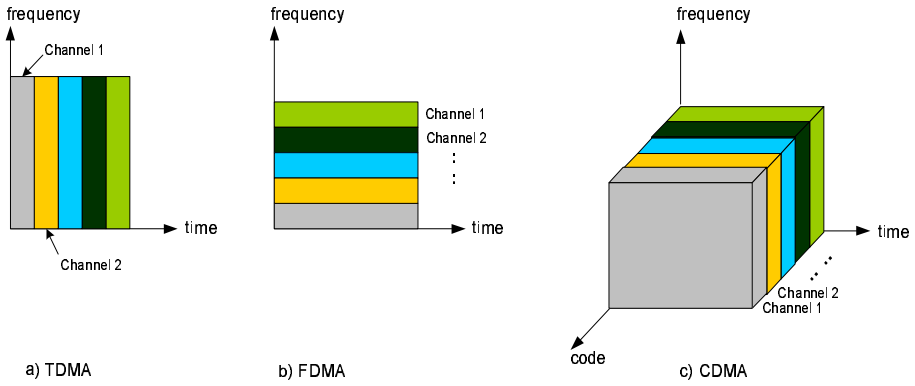

Figure 3.1: Multiple access schemes: TDMA, FDMA and CDMA [30]

for part of the time results in Time Division Multiple Access (TDMA) [28]. Division by frequency, so that each pair of communicators is allocated part of the spectrum for all of the time, results in Frequency Division Multiple Access (FDMA) [28]. In CDMA, every communicator will be allocated the entire spectrum all of the time. In CDMA, all users can use the same bandwidth at the same time, but they can now be separated by PRN codes assigned to each user [28]. The PRN codes are chosen to be like random noise but still deterministic [1]. The current TDMA and FDMA systems are considered as narrowband systems, since the idea behind these is to use as narrow transmission band for one user as possible. The objective is to allocate a minimum amount of fixed RF spectrum for each user. The narrower is the bandwidth per user, the more users can be served by the fixed RF spectrum. On the contrary, in CDMA system, the basic idea is to spread the narrowband data signal over a wider bandwidth using the pseudorandom code, i.e., the spreading code. In CDMA, the bandwidth is thus traded for capacity.

3.2 Spread Spectrum System

The most common spread spectrum system is shown in Figure 3.2 . Formally, the operation

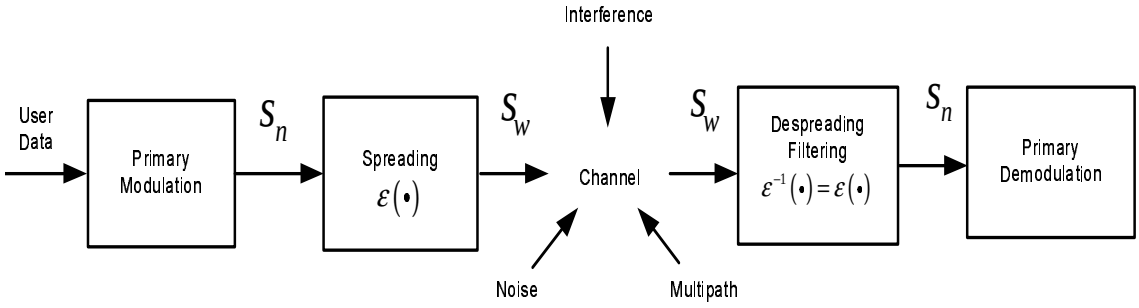

Figure 3.2: Spread spectrum system concept [29]

of both transmitter and receiver is partitioned into two steps. In the first step, which is

referred to as primary modulation, the narrowband signal S_n is formed. The narrowband signal is then fed into the second step where the spreading operation $\varepsilon(\cdot)$ is performed resulting in the expansion of the signal spectrum to a very wide frequency band. This transmitted signal is denoted by S_w. [29]

On the receiver side, the despreading operation converts the received wideband signal into a narrowband signal, which is then demodulated by traditional means. For convenience, it is assumed that the despreading operation is identical to the spreading operation, i.e., $\varepsilon^{-1}(\cdot) = \varepsilon(\cdot)$ as shown in Figure 3.2. [29]

3.3 Spreading Methods

There are several spreading techniques explained in the literature to spread a signal: Direct Sequence (DS), Frequency Hopping (FH), Time Hopping (TH) and Multi-Carrier (MC) CDMA. An overview of these spread spectrum techniques can be found in [27, 31, 32, 33, 34, 35]. We will only focus on DS technique in what follows because this is the multiple access technique used in GNSS systems.

The DSSS system is the most encountered spread spectrum technique. In DSSS, each narrowband bit or symbol is replaced by a sequence of shorter symbols called 'chips'. The chip rate is much larger than the information signal bit rate. Each information bit of a digital signal is transmitted as a PRN sequence of chips. The DSSS system is also called pseudonoise system, since the multiplying signal consists of PRN sequences [36].

3.4 CDMA

In CDMA systems, all users transmit in the same bandwidth simultaneously. In this transmission technique, the frequency spectrum of a data-signal is spread using a code uncorrelated with that signal. As a result the bandwidth occupancy is much higher than required. The codes used for spreading have low crosscorrelation values and are unique to every user. This is the reason that a receiver which has knowledge about the code of the intended transmitter, is capable of receiving the desired signal. [28]

CDMA can be classified into three different modulation methods: Frequency Hopping CDMA (FH-CDMA), Time Hopping CDMA (TH-CDMA) and Direct Sequence CDMA (DS-CDMA). DS-CDMA is the most widely used among the above mentioned modulation methods. The GPS and Galileo systems also use DS-CDMA method, which will be the focus in what follows.

3.5 Spreading Codes

In a DS-CDMA system, the data signal is multiplied with a spreading code in the transmitter, and despread with the same spreading code in the receiver in order to find out the original data. In the satellite navigation systems, each satellite has a unique PRN spreading code. Despreading diminishes the interference from other users, and hence, the DS-CDMA technique allows multiple users to use the same bandwidth simultaneously. Despreading is performed via correlation, which measures the similarity of two signals. In order to be able to separate different users, the PRN spreading codes should have very low crosscorrelation. This means that in an ideal case, the codes are orthogonal and have zero correlation with other codes used in the system. On the other hand, codes should have good (impulse-like) autocorrelation properties, i.e., code should correlate with itself, in order to be able to detect a delayed (i.e., time shifted) signal [29]. Correlation is a fundamental operation in the signal tracking process, where the timing of the arriving signal is determined. [28]

A spreading code consists of a number of code symbols called chips. The rate of the spreading code is called chip rate f_{chip} (code symbols per second) and it should be higher than the bit rate R (bits per second) of the data signal in order to achieve desired spreading. Spreading factor (S_F) is typically defined as the ratio between the chip rate and the bit rate [28], [37]:

$$S_F = \frac{f_{chip}}{R}$$

Spreading codes can be divided into short and long codes. Short code spans over one data symbol interval, which means that the spreading code of a certain user remains the same for all data symbols. Respectively, long codes span over several data symbol periods. Short codes are usually used to control the correlation properties or reduce the system complexity. Long codes are noticed to reduce the interference. Short codes are used, e.g., for GPS C/A signals [1]. The first Galileo test satellite Giove-A was launched on December'2005. Giove-A L1 signal has two spreading codes where both the codes are truncated gold codes [38].

3.6 Pros and Cons of DS-CDMA System

Besides the more effective use of the transmission band and multiple access capability, spreading the information to wider bandwidth produces also other advantages to the system. The major benefits of DS-CDMA system are listed below:

- Low power spectral density: less interference to other systems and possibility to re-use spectrum by overlay systems (anti-jamming and anti-interference)
- Reliable transmission in multipath fading channels via the rake receiver [37, 39, 40]
- Low probability of interception (military applications)
- Multiple user random access communications with selective addressing capability (i.e., CDMA with multiple users) [37]

DS-CDMA has been chosen to be the popular transmission technique for many digital mobile systems due to the advantages mentioned above. On the other hand, a DS-CDMA system cannot work without successful synchronization between the received signal and the replica spreading code. Therefore, the acquisition and tracking of the correct code phase and frequency shift are fundamental prerequisites for any DS-CDMA system. Another possible drawback of the DS-CDMA technology is the Multiple Access Interference (MAI), which is usually a challenge in the wireless communication systems, because the code orthogonality is destroyed by the multipath channel [29]. MAI has not been considered to be a serious problem in GNSS systems, but with increasing number of satellites in the same frequency band and increasing interest in positioning with severe multipath channels, MAI may become a challenge also in this context [41].

Chapter 4

Fading Channel Model

The wireless channel can be described as a function of time and space, and the received signal is the combination of many replicas of the original signal impinging at receiver from many different paths [42, 43, 44, 45]. The component signals on these different paths can constructively or destructively interfere with each other. This is referred as multipath. If either the transmitter or the receiver is moving, then this propagation phenomena will be time varying, and fading occurs. The behavior of a typical wireless fading channel is considerably more complex to deal with than that of an Additive White Gaussian Noise (AWGN) channel. Besides the thermal noise at the receiver front end (which is modeled by AWGN), there are several other well-studied channel impairments in a typical wireless channel: *propagation attenuation* or *path loss*, *shadowing* and *fading* [42, 43, 45]. A brief introduction on these three impairments is given in section 4.2. The main focus is on multipath fading, especially on Rayleigh distributed fading. However, this chapter offers a brief overview of wireless fading channel models and the challenges caused by signal propagation and by the movement of the receiver.

4.1 Propagation Environments

The quality of the received signal depends on the propagation channel. From the positioning point of view, in an optimal transmission channel, there is a direct LOS path between the transmitter and the receiver. This means that the signal arrives straight to the receiver via the shortest possible path without any reflections. However, if the receiver, e.g., a Mobile Station (MS), is behind an obstacle or inside a building, the LOS path may be absent and the arriving signal can be diffracted, reflected, or scattered. This situation is known as Non-LOS (NLOS) scenario. [28, 46]

The propagation environments have been divided into several different environment types. One division can be made between indoor and outdoor cases. In indoor scenario, the

receiver is inside a building and typically the speed of the receiver is very low. Outdoor scenarios consist of microcellular and macrocellular areas. If the receiver antenna is below the buildings' average rooftop level, the environment is typically defined as microcellular. In microcellular areas, both LOS and NLOS communications are possible. Macrocellular areas can be further divided into urban, suburban or rural areas, depending on the building density (e.g., city or small village) and on the type of vegetation (e.g., forest or field). This classification is generally used in mobile communications, but it can also be applied for satellite-based positioning. [28, 46]

4.2 Channel Impairments

In order to fully understand wireless communications, a basic idea on the characteristics of wireless channels is a must. The channel characteristics can be mostly described by path loss, shadowing and fading. Therefore, a brief introduction on these channel impairments is provided in what follows.

4.2.1 Path Loss

In any real channel, signals attenuate as they propagate. For a radio wave transmitted by a point source in free space, the loss in power, known as path loss, is given by: [42, 43]

$$L = \left(\frac{4\pi d}{\lambda}\right)^2, \tag{4.1}$$

where λ is the wavelength of the signal, and d is the distance between the source and receiver. The power of the signal decays as the square of the distance.

4.2.2 Shadowing

Shadowing is due to the presence of large-scale obstacles in the propagation path of the radio signal. Due to the relatively large obstacles, movements of the mobile units do not affect the short-term characteristics of the shadowing effect. Instead, the natures of the terrain surrounding the receiver generally determine the shadowing behavior. [43, 45]

Shadowing is modeled as a slowly time-varying multiplicative random process. Neglecting all other channel impairments, the received signal $r(t)$ is given by:

$$r(t) = g(t)s(t) \tag{4.2}$$

where $s(t)$ is the transmitted signal and $g(t)$ is the random process which models the shadowing effect. For a given observation interval, g(t) can be assumed as a constant g,

which is usually modeled as a log normal random variable whose density function is given by:

$$p(g) = \begin{cases} \frac{1}{\sqrt{2\pi}\sigma g} \exp\left(-\frac{(\ln g - \mu)^2}{2\sigma^2}\right) & g \geq 0 \\ 0 & g < 0, \end{cases} \tag{4.3}$$

where $\ln g$ is a Gaussian random variable with mean μ and variance σ^2. This translates to the physical interpretation that μ and σ^2 are the mean and variance of the loss measured in decibels (up to a scaling constant) due to shadowing.

4.2.3 Fading

Fading is the term used to describe the fluctuations in the envelope of a transmitted radio signal. Fading is a common phenomenon in wireless communication channels caused by the interference between two or more versions of the transmitted signals which arrive at the receiver at slightly different times. The resultant received signal can vary widely in amplitude and phase, depending on various factors such as the intensity, relative propagation time of the waves and bandwidth of the transmitted signal [42, 43]. The performance of a DS-CDMA system can be severely degraded by fading. In literature, there exist different types of fading channel models, namely, Rician, Rayleigh and Nakagami channel models which are characterized by Rician, Rayleigh and Nakagami distributions, respectively. These fading distributions are discussed briefly in section 4.5. The simulation model in this thesis does not incorporate path loss and shadowing.

4.3 Fading Channel Parameters

Fading channel parameters are often used to characterize a fading channel. Therefore, a brief discussion on fading channel parameters is presented in this section.

4.3.1 Delay Spread

Suppose that a very narrow pulse is transmitted in a fading channel. The received power can be measured as a function of time delay. The average received power $P(\tau_e)$ as a function of the excess time delay τ_e (excess time delay = time delay - time delay of first path) is called the multipath intensity profile or the delay power spectrum. The range of values of τ_e over which $P(\tau_e)$ is essentially non-zero is called the multipath delay spread of the channel, and is often denoted by T_m. It essentially tells the maximum delay between paths of significant power in the channel.

4.3.2 Coherence Bandwidth

In a fading channel, signals with different frequency contents can undergo different degrees of fading. Coherence bandwidth, denoted by $(\Delta f)_c$, is a statistical measure of the range of frequencies over which the channel can be considered flat. In other words, coherence bandwidth can be considered as the approximate maximum bandwidth or frequency interval over which two frequencies of a signal are likely to experience comparable or correlated amplitude fading. Therefore, if two sinusoids are separated in frequency by more than $(\Delta f)_c$, then they would undergo different degrees of (often assumed to be independent) fading. It can be shown that $(\Delta f)_c$ is related to multipath delay spread T_m by: [43, 45]

$$(\Delta f)_c \approx \frac{1}{T_m} \tag{4.4}$$

4.3.3 Coherence Time

In a time-varying channel, the channel impulse response varies with time. The coherence time, denoted by $(\Delta t)_c$, gives a measure of the time duration over which the channel impulse response is essentially invariant (or highly correlated) [43, 45]. Therefore, if a symbol duration is smaller than $(\Delta t)_c$, then the channel can be considered as time invariant during the reception of a symbol. Of course, due to the time-varying nature of the channel, different time-invariant channel models may still be needed in different symbol intervals.

4.3.4 Doppler Shift and Doppler Spread

The movement of the satellite in comparison with the GNSS receiver creates some frequency shift to the code and carrier frequencies of the received signal [1]. This phenomenon is called Doppler effect and the frequency shift is known as Doppler shift f_D. Since Doppler shift is dependent on the satellite speed, a single received signal will have a maximum Doppler frequency shift of: [29, 43, 45]

$$f_D = \frac{v_s f_c}{c}, \tag{4.5}$$

where v_s is the speed of the satellite, f_c is the carrier frequency and c is the speed of light. Due to the multipath propagation and the mobile speed of the receiver, the arriving signal components are different at each moment and hence, there is some small variation in the Doppler shift of the received signal [1]. Doppler spread $(\Delta f)_{ds}$ defines the possible range of the Doppler shift due to the mobile speed, and its maximum value can be calculated as: [1]

$$(\Delta f)_{ds} = \frac{v_m f_c}{c}, \tag{4.6}$$

where v_m is the mobile speed of the receiver. Doppler spread $(\Delta f)_{ds}$ is inversely related to coherence time $(\Delta t)_c$.

4.4 Classification of Fading Channel

As explained in section 4.2.3, the general term fading is used to describe the fluctuations in the envelope of a transmitted radio signal. However, when speaking of such fluctuations, it is of interest to consider whether the observation has been made over short distances or long distances. For a wireless channel, the former case will show rapid fluctuations in the signal's envelope, while the latter will give a more slowly varying, averaged view. For this reason, the first scenario is formally called small-scale or multipath fading, while the second scenario is referred to as large-scale fading or path loss [47]. Small-scale fading is explained by the fact that the instantaneous received signal strength is a sum of many contributions coming from different directions due to the many reflections of the transmitted signal reaching the receiver [43]. Since the phases are random, the sum of contributions varies widely. The amplitude of the received signal typically obeys a Rayleigh fading distribution. In small-scale fading, the received signal power may vary by as much as three or four orders of magnitude (30 or 40 dB) when the receiver is moved on the order of only a fraction of a wavelength [47]. Large-scale fading is explained by the gradual loss of received signal power (since it propagates in all directions) with transmitter-receiver separation distance [43].

Small-scale fading occurs as either of 4 types, namely, i. *frequency selective fading*, ii. *flat fading*, iii. *fast fading* and iv. *slow fading* [43]. A brief overview of these fading types is presented in what follows.

4.4.1 Frequency Selective Fading

Fading resulting from multipath propagation varies with frequency since each frequency arrives at the receiving point via a different radio path. When a wide band of frequencies is transmitted simultaneously, each frequency will vary in the amount of fading. This variation is called frequency selective fading. In frequency selective fading, the transmitted signal has a bandwidth B_W greater than the coherence bandwidth $(\Delta f)_c$, i.e., $B_W > (\Delta f)_c$ and the delay spread T_m is greater than the symbol period T, i.e., $T_m > T$. When frequency selective fading occurs, all frequencies of the transmitted signal do not retain their original phases and relative amplitudes. This fading causes severe distortion of the signal and limits the total signal transmitted. [43, 45]

4.4.2 Flat Fading

The wireless channel is said to be flat fading if it has constant gain and linear phase response over a bandwidth which is greater than the bandwidth of the transmitted signal

[42, 43, 48]. In other words, flat fading occurs when the bandwidth of the transmitted signal B_W is much smaller than the coherence bandwidth of the channel $(\Delta f)_c$, i.e., $B_W << (\Delta f)_c$ [49]. In flat fading, multipath delay spread T_m is less than the symbol period T, i.e., $T_m < T$ [48].

4.4.3 Fast Fading

Fast fading occurs if the channel impulse response changes rapidly within the symbol duration [42, 43, 48]. In other words, fast fading occurs when the coherence time of the channel $(\Delta t)_c$ is smaller than the symbol period of the transmitted signal T such that $(\Delta t)_c < T$. This causes frequency dispersion or time selective fading due to Doppler spreading [48]. Fast fading is due to reflections of local objects and the motion of the objects relative to those objects.

4.4.4 Slow Fading

Slow fading is the result of shadowing by building, mountains, hills and other objects [50]. In slow fading channel, the symbol period T is less than the channel coherence time $(\Delta t)_c$, i.e., $T < (\Delta t)_c$, which is opposite to the situation in fast fading channel [48]. Since the coherence time is in relation to the Doppler spread, it can be concluded that the speed of the receiver determines whether the fading for the transmission channel is fast or slow [39].

4.5 Fading Distributions

In the thesis, the discrete linear time-variant model for the channel impulse response is used. The motivation came from the fact that linear models are much simpler to simulate and analyze than the nonlinear ones. Moreover, the channel modeling with a finite number of taps is more convenient and natural for computer simulations and has been proved to cover a multitude of wireless propagation scenarios [28, 51]. Several nonlinear fading channel models have also been proposed in the literature which usually fall in two categories: i. models based on expanding the nonlinear characteristics into a power series [52, 53] and ii. Markov chain models [54, 55].

Fading phenomenon can be modeled via the so called fading channel coefficients for linear time-variant model, which reflect the severity of the fading phenomenon. Depending on the the environment of the signal propagation, these coefficients follow different distribution models. When the multipath fading has direct LOS signal, the fading distribution of the received signal is typically assumed to be Rician. However, in case of a NLOS situation,

the received signal fading typically follows a Rayleigh distribution [56]. This distribution is used to characterize dense urban area or indoor environments. The third distribution type which is presented in this section is Nakagami-m. The Nakagami-m distribution, which has been used to model the satellite-to-indoor mulipath propagation [57, 58], spans the range from one sided Gaussian fading ($m = 1/2$) to the non-fading AWGN channel ($m \to \infty$).

4.5.1 Rician Distribution

In the case of at least one strong LOS signal path and possible severe weaker NLOS paths, the fading channel distribution is Rician [56]. The amplitude α of the fading channel follows the distribution of: [59]

$$p_\alpha(\alpha) = \frac{2(1+n^2)e^{-n^2}\alpha}{\Omega} \exp\left(-\frac{(1+n^2)\alpha^2}{\Omega}\right) I_0\left(2n\alpha\sqrt{\frac{1+n^2}{\Omega}}\right), \tag{4.7}$$

where $\alpha \geq 0$, Ω is average fading power, $I_0(\cdot)$ is the modified Bessel function of the first kind and zero-th order, and n^2 is the Rician factor, often denoted by K ($K = n^2$).

In Rician fading, the in-phase and quadrature phase components of the received signal are independent identically distributed joint Gaussian random variables. However, in Rician fading the mean value of (at least) one component is non-zero due to a deterministic strong wave.

4.5.2 Rayleigh Distribution

Rayleigh fading is a reasonable model when there are many objects in the environment that scatter the radio signal before it arrives at the receiver. If there is sufficiently much scatter, the channel impulse response will be well-modelled as a Gaussian process irrespective of the distribution of the individual components. If there is no dominant component to the scatter, then such a process will have zero mean and phase evenly distributed between 0 and 2π radians [60]. The power, or envelope, of the channel response will therefore be Rayleigh distributed. Rayleigh fading is more severe than Rician fading, which means that the fading fluctuations are deeper [28]. In the case of NLOS propagation paths, Rayleigh distribution is likely to fit quite well for the measured data [61]. For Rayleigh fading, the channel phases are uniformly (randomly) distributed [37] and the channel fading amplitudes are distributed according to: [59]

$$p_\alpha(\alpha) = \frac{2\alpha}{\Omega} \exp(-\frac{\alpha^2}{\Omega}), \tag{4.8}$$

where $\alpha \geq 0$. Rayleigh is a special case of Rice distribution [59] and Rayleigh fading is a small-scale effect.

4.5.3 Nakagami-m Distribution

Nakagami distribution, also named m-distribution, is an important distribution as a generic model of fade statistics used in the study of mobile radio communications [59, 62]. A Wide class of fading channel conditions can be modeled with Nakagami-m distribution [59]. This fading distribution has gained a lot of attention lately, since the Nakagami-m distribution often gives the best fit to land-mobile and indoor mobile multipath propagation as well as scintillating ionospheric radio links [56]. More recent studies also showed that Nakagami-m gives the best fit for satellite-to-indoor radio wave propagation [57, 58].

Nakagami-m distribution can be defined as: [56]

$$p_\alpha(\alpha) = \frac{2m^m \alpha^{2m-1}}{\Omega^m \Gamma(m)} \exp\left(-\frac{m\alpha^2}{\Omega}\right), \tag{4.9}$$

where $\alpha \geq 0$, $\Gamma(\cdot)$ is gamma function and m is the Nakagami fading parameter. The value for m can range between $1/2$ and ∞. When $m \to \infty$, the channel begins to converge to a static channel. As special cases, Nakagami-m follows Rayleigh distribution if $m = 1$, and for $m = 1/2$ the distribution corresponds to one-sided Gaussian. This means that, if the value of m is less than 1, the Nakagami distribution is more severe than Rayleigh, and for values of m higher than 1, the fading circumstances are lighter. For the values of $m > 1$, the Nakagami-m distribution closely approximates the Rician distribution, and the parameters m and n^2 can be mapped via equation of $m = \frac{(1+n^2)^2}{1+2n^2}$, when $n \geq 0$. [59]

4.6 Carrier-to-Noise-Ratio

Both in static and fading channels, the transmitted signal is affected by complex additive white Gaussian noise. CNR is in relation to the ratio between the bit energy E_b and the noise variance N_0, and it can be calculated in dB-Hz as follows:

$$CNR_{dB-Hz} = 10\log_{10}(B_W) + \frac{E_b}{N_0}, \tag{4.10}$$

where B_W is the signal bandwidth after despreading and E_b/N_0 is given in dB. From now on, CNR_{dB-Hz} in dB-Hz is denoted simply by CNR.

Chapter 5

Code Synchronization in DS-CDMA Systems

In spread spectrum systems, it is essential to estimate the timing and frequency shift of the received signal in order to be able to despread the received signal and to demodulate the despread signal. This process is called code synchronization and usually contains the following two steps: [1]

- **Code acquisition** (coarse acquisition or coarse synchronization) synchronizes the transmitter and receiver to within a delay uncertainty of $\pm T_c$, where T_c is the chip duration, and a frequency uncertainty of ± 0.5 KHz.
- **Code tracking** performs and maintains fine synchronization between the transmitter and the receiver.

The basic code synchronization procedure for DS-CDMA systems is shown in Figure 5.1. In Figure 5.1, code acquisition provides a coarse estimate of the code delay τ_{acq} followed by code tracking stage where the objective is to estimate the correct code delay $\hat{\tau}$.

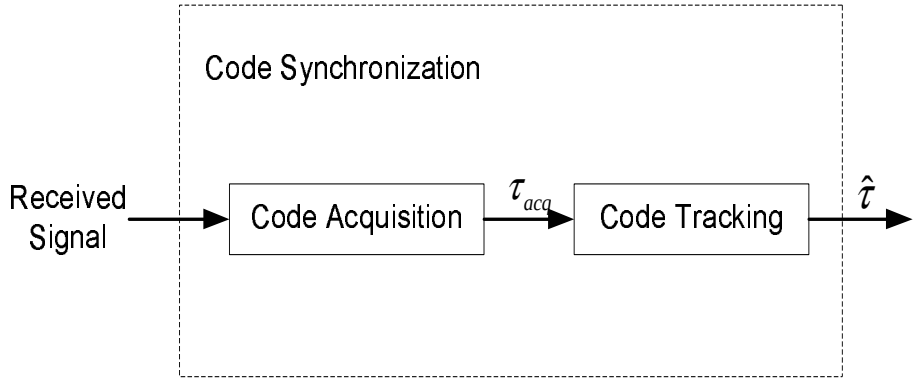

Figure 5.1: Basic code synchronization procedure and its output

5.1 Code Acquisition

The objective of code acquisition is to achieve a coarse synchronization between the received signal and the replica spreading code [63]. In this stage, both code estimation and frequency estimation have to be performed. Therefore, the signal acquisition process consists of two stages, namely **the search stage** and **the detection stage** in order to estimate both code delay and frequency shift [64]. These two stages are briefly described in this section.

5.1.1 Search Stage

The basic idea of the search strategy is to define the position where there is an alignment between the received signal and the spreading code [64]. The process is done using cross-correlation, which measures the similarity of the code and the delayed replica of the same code. The search process is usually two-dimensional by which both the time shift (i.e., delay) and Doppler shift have to be determined [1]. The value of the Doppler shift changes over time according to the place and speed of the satellite. Therefore, it is important from the acquisition point of view to know the possible value of the Doppler frequency. It is naturally much more easier to look for the correct frequency, if the Doppler shift can be estimated in advance (i.e., aided acquisition) [41].

Search Space

In the search process, all possible code delays and frequencies are searched through with some predefined search steps. The search space is typically equal to the length of the spreading code in the code-delay domain. In the Doppler frequency domain, the search interval can be several kHz or even tens of kHz [65]. If some *a priori* information (i.e., assistance data) about the Doppler frequency is available, the frequency interval may be just few tens of Hz [65].

Search Window

Each tentative code phase is called a code bin (or a time bin) and respectively each tentative frequency shift is denoted as a Doppler bin (or a frequency bin). One code bin together with one Doppler bin compose a search bin (or a test cell). The whole code-frequency uncertainty region can be divided into several search windows and each window can be divided into several time-frequency bins. The time-frequency search window defines the decision region. [1]

Search Strategy

In the search stage, the search windows are examined to see whether the time-frequency estimate is correct or not. The search process is started from one search window, with a certain tentative Doppler frequency and a certain tentative delay. All delays and frequencies, which correspond to the size of the search window at issue, are searched through with the predefined searched steps. If the window is decided to be dismissed, the search process moves on to the next search window, and the same procedure is continued, until the correct window and the correct delay-frequency combination is found. [1, 64]

Correlation

The tentative time-frequency bins are tested and possible signals are detected via cross-correlation. This means that the received signal is correlated with the reference code with different tentative delays and frequencies, and the resulting values are then combined to achieve a two-dimensional correlation output for the whole search window. From the correlation output, it can be further determined whether the search window is correct or not via a correlation peak which appears for correct delay-frequency combination. The correlation process is described in detail in [1, 41].

Search Algorithms

PRN codes proposed for Galileo systems have higher lengths (e.g., 4092 chips for L1F signals and 10230 chips for E5 signals [17]) than those used in traditional GPS. Obviously, longer codes lead to an increased search space or uncertainty region, and hence, the search process is getting more time consuming [41]. Several search algorithms have been developed in order to obtain faster and more efficient signal acquisition, namely **serial search**, **parallel search** and **hybrid search** [41, 66].

In **serial search**, the search window consists of only one bin and the delay shift is changed by steps of one time-bin length. Thus, all time bins are examined one by one in a serial manner and only one search detector is needed for the acquisition [41]. Since the received signal is complex, one search detector contains in fact two real correlators, one for the I-branch and the other for the Q-branch of the complex signal [63]. Since the time-frequency bins are tested one at a time in the serial search approach, the search process may take very long time if the uncertainty region is large. For this reason, the serial search strategy is mostly used if there is some assistance information available about the correct Doppler frequency and the correct code delay [64].

A **parallel search** strategy uses a bank of matched filters, each matched to a different waveform pattern of PRN code subsequences corresponding to all possible PRN code phases and all possible Doppler bins, and then make a decision based on all the outputs of the filters [66]. In fully parallel search, the acquisition scheme simultaneously test all possible code phases and all possible Doppler bins, therefore, it can significantly reduce the code acquisition time [66]. Obviously, the acquisition time is considerably smaller, but at the same time the complexity increases, since more correlators are needed [67].

A **hybrid search** strategy is a trade off between the parallel and serial search strategies, it allows to achieve a proper balance between the acquisition speed and the hardware complexity and it covers the serial- and parallel-search situations as two extreme cases, as explained in [66, 68]. In the hybrid search strategy, the number of bins per window is however still limited by the available number of correlators [69, 70].

5.1.2 Detection Stage

The simplified block diagram of code acquisition technique is depicted in Figure 5.2. After the correlation between the received signal and the locally generated reference code, acquisition continues with coherent integration over N_C chips (coherent integration period or coherent integration length), where the I- and Q-branches of the complex signals are Integrated and Dumped (I&D) to form correlation output. Integration is performed by the I&D -block in Figure 5.2, which acts as a low pass filter as well, by removing higher

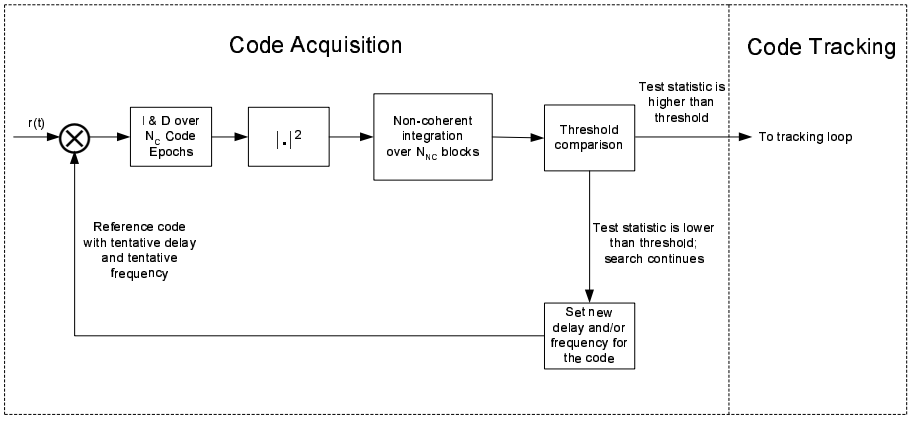

Figure 5.2: Simplified Block Diagram of Code Acquisition Technique

frequency components from the signal. Coherent integration is further followed by non-coherent integration over N_{NC} blocks (non-coherent integration length). Non-coherent integration is used here to decrease the noise floor and also because the coherent integration time N_C might be limited by the channel fading, Doppler [39] and by the instability of the oscillator clocks. The next step is to define if the signal is present or absent, i.e.,

if there is a synchronization between the code and the received signal or not. This is the aim of the detection stage. [1, 71]

Detection Probability

In the detection stage, a test statistic is computed per each search window, based on the current correlation output, and then this test statistic is compared to a certain predetermined threshold γ in order to decide whether the signal is present or absent. The test statistic can be formed, for example, as the value of the global maximum of the correlation output in one search window [56, 65], or as the ratio between the global maximum and the next significant local maximum [72, 73]. If the value of the test statistic is higher than the threshold, the signal is decided to be present and an estimate for the code phase and frequency is achieved. The time to form the test statistic is usually denoted as the dwell time τ_d. Every time when the test statistic is higher than the threshold, the signal is decided to be present. The probability of a signal being detected correctly is denoted as a detection probability P_d. [1]

False Alarm Probability

False alarm situation happens if a delay and/or frequency estimate is wrong but the test statistic is still higher than the threshold, i.e., the signal is declared present in an incorrect window. The probability of a false alarm case is denoted as false alarm probability P_{fa}. It may also happen that the signal is present, but not detected: a miss detection occurs. This may happen if the threshold is set too high or the environment is so noisy that the signal is lost into the background noise. [1, 74]

Detection Threshold

The choice of a suitable detection threshold γ has a significant role in the acquisition process. If the threshold is set too low, the probability of detection (i.e., P_d) naturally increases, but at the same time, the probability of false alarm (i.e., P_{fa}) increases as well. Respectively, if the threshold is set too high, the P_{fa} decreases, but also the P_d is low. The selection of a suitable detection threshold is explained, for example, in [41].

5.2 Code Tracking

A code tracking loop starts its operation only after initial acquisition has been achieved. In the code acquisition process, the normalized delay error between the input signal and

the locally generated replica code, $\delta = (\tau - \hat{\tau})/T_c$ is reduced to the range $\delta < 1$ chip, where T_c is the chip duration. The objective of the code tracking loop is to further reduce this error down to zero and then to track any changes in code delay (i.e., τ). This loop structure is well-known as Delay Lock Loop or Delay Locked Loop (DLL) [29]. There are several delay tracking loop structures, DLL is only one of them and is the focus area of the thesis.

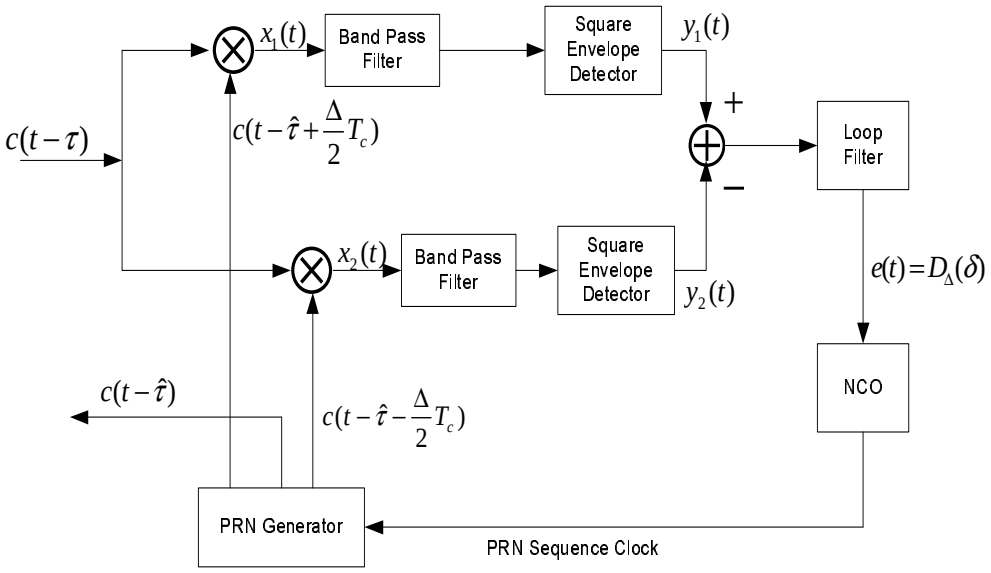

Figure 5.3: Simplified block diagram of a conventional non-coherent DLL [29]

A conceptual simplified block diagram of a conventional non-coherent DLL is shown in Figure 5.3. In a conventional non-coherent DLL as presented in Figure 5.3, the input signal is correlated with two locally generated, mutually delayed early and late replicas of the PRN code [29]. The spacing between early and late replicas is denoted as Δ. The DLL spacing (i.e., Δ) has significant impact on the performance of the discriminator-based DLL algorithms which is described in section 6.2. Referring to Figure 5.3, the results of the late correlator and the early correlator pass through a Band Pass Filter (BPF) and a square envelope detector. There difference produces an error signal $e(t)$. The error signal applies to a loop filter and the Numerically Controlled Oscillator (NCO) which drives the PRN sequence generator to correct timing. The discriminator function (i.e., $D_\Delta(\delta)$) in this example case can be represented as:

$$D_\Delta(\delta) = \left|R(\delta + \frac{\Delta}{2})\right|^2 - \left|R(\delta - \frac{\Delta}{2})\right|^2, \tag{5.1}$$

where $R(\delta)$ is the autocorrelation of the sequence. This is one of the most common structures based on two correlators known as Early Minus Late (EML) correlator. There are different discriminator-based DLL algorithms which differ in terms of varying chip spacing

as well as varying the number of correlators used to form the discriminator function. The discriminator based algorithms are discussed in Chapter 6.

Several types of DLL have been proposed in the literature for code tracking. Mainly, there are two types of DLL: **non-coherent** and **coherent** [75, 76]. Non-coherent DLL uses nonlinear devices (such as squaring or absolute value) in order to remove the effect of data modulations and channel variations [75]. On the contrary, coherent DLL does not suffer from squaring losses and gain imbalances [77, 78]. However, non-coherent DLL is used in the thesis work as it is of interest in DS-CDMA systems where code acquisition and tracking must be performed prior to obtaining carrier synchronization.

The performance of a DLL is well-characterized by the so-called S-curve, which presents the expected value of the the error signal as a function of the reference parameter error (i.e., the code mismatch) [29, 31, 76]. The mathematical definition of the S-curve for DLL is given in equation 5.1. The intuition behind the S-curve is the fact that searching for maxima in the correlation function is equivalent with finding the zeros of the gradient, which can be approximated by first-order differences [75].

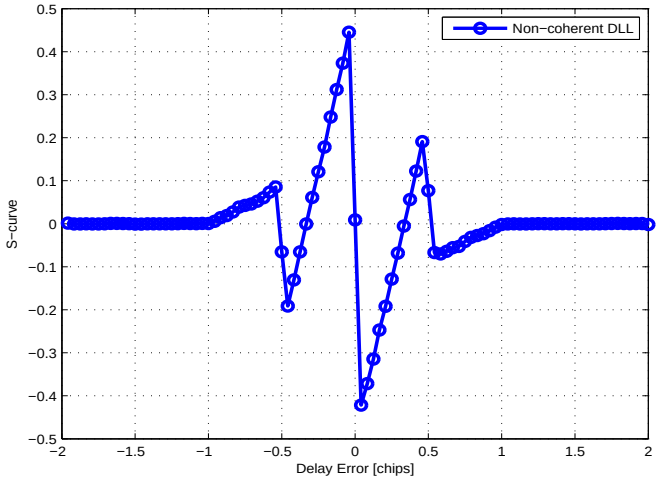

Figure 5.4: S-curve for non-coherent DLL in single path Rayleigh fading channel model

Figure 5.4 represents one example S-curve for non-coherent DLL in single path Rayleigh fading channel model with average tap power 0 dB. In this example case, the delay of the LOS path can be estimated by finding the zero crossing from above to below. As it can be noticed from Figure 5.4 that there are some false lock points at about ± 0.5 chips. This is due to fact that the ACF of SinBOC(1,1) modulated signal has side lobe peaks at ± 0.5 chips. This situation is even more challenging in the presence of randomly separated multipaths. This is still an open research issue to deal with the false lock points, especially in multipath fading channel models. However, as mentioned in [75], DLL-based

techniques have reduced ability to deal with closely spaced path scenarios under realistic assumptions (such as presence of errors in the channel estimation process) as well as have the possibility to lose the lock (i.e., start to estimate the delays with high estimation error) due to feed-back error propagation.

Chapter 6

Code Tracking Algorithms

In general, the tracking algorithms can be grouped into two main categories: **feed-back technique** and **feed-forward technique** [75, 79]. Code tracking algorithms based on feed-back technique form a discriminator function at the receiver, find a delay estimate based on the discriminator, and feed it back in the loop so that it could be used in the following delay estimation. The most known feed-back structures are also known as DLLs [9, 80, 81, 82, 83]. The feed-back code tracking algorithms which are analyzed in the thesis are mentioned below:

- Wide Correlator
- Narrow Correlator
- High Resolution Correlator
- Multiple Gate Delay Correlator

On the contrary, feed-forward technique is based on a threshold computation which should be determined according to channel condition [75, 79]. In the thesis, the following feed-forward code tracking algorithms are analyzed:

- Multipath Estimating Delay Lock Loop
- Differential Order 2 Scheme
- Matched Filter

It is the general belief that feed-forward technique is more complex than the feed-back technique due to a higher number of correlators (usually needed) and to some additional processing that might be needed at the receiver. However, it is also possible to combine

feed-back with feed-forward delay estimation so that the combined approach can utilize the advantages from both the techniques. One such algorithm is proposed herein which is the main focus area of the thesis. PT is the proposed novel algorithm which combines both feed-back and feed-forward techniques and utilizes the statistical properties of the correlation function in the process of delay estimation. This new algorithm is extensively compared with the existing feed-back and feed-forward algorithms mentioned earlier. The simulation results are presented in Chapter 8. All the above mentioned code tracking algorithms are discussed in what follows whereas the new PT algorithm is described in detail in the following chapter.

6.1 Wide Correlator

The classical tracking structure for spread spectrum systems is the wide correlator, where two correlators spaced at $\Delta_{WEML} = 1$ chip from each other are used in the receiver to form a discriminator function, whose zero crossings determine the multipath delays [84, 85]. On the basis of autocorrelation function introduced in Figure 6.1, the corresponding EML code discriminator of SinBOC(1,1) modulated signal can be computed. The wide correlator or Wide EML (WEML) is computed by subtracting an early and a late version of the correlation function illustrated in Figure 6.1, using a chip spacing of 1 chip. We remark that a zero crossing from below corresponds here to the correct delay. Then a discriminator function D_{WEML} is formed of the type:

$$D_{WEML}(\tau) = \left| R(\tau + \frac{\Delta_{WEML}}{2}) \right|^2 - \left| R(\tau - \frac{\Delta_{WEML}}{2}) \right|^2, \tag{6.1}$$

where $R(\tau)$ is the ACF of the received signal and auto-generated replica code, and Δ_{WEML} is the early-late chip spacing for wide EML.

6.2 Narrow Correlator

A first approach to reduce the influences of code multipath is the narrow correlation or Narrow EML (NEML) technique, which was first proposed in 1992 [84, 86, 87]. This technique has been introduced to GPS receivers by NovAtel. Instead of using a wide correlator with a chip spacing of 1 chip between early and late code, the chip spacing of a narrow correlator is less than 1 chip, i.e., $\Delta_{NEML} < 1$ chip. Correlator spacings of 0.1 or 0.05 chips are commercially available for GPS. The narrow correlator uses the same discriminator function as like wide correlator; the only difference between wide and narrow correlator is the chip spacing used to compute the above mentioned discriminator function. The discriminator function for non-coherent narrow correlator is given below:

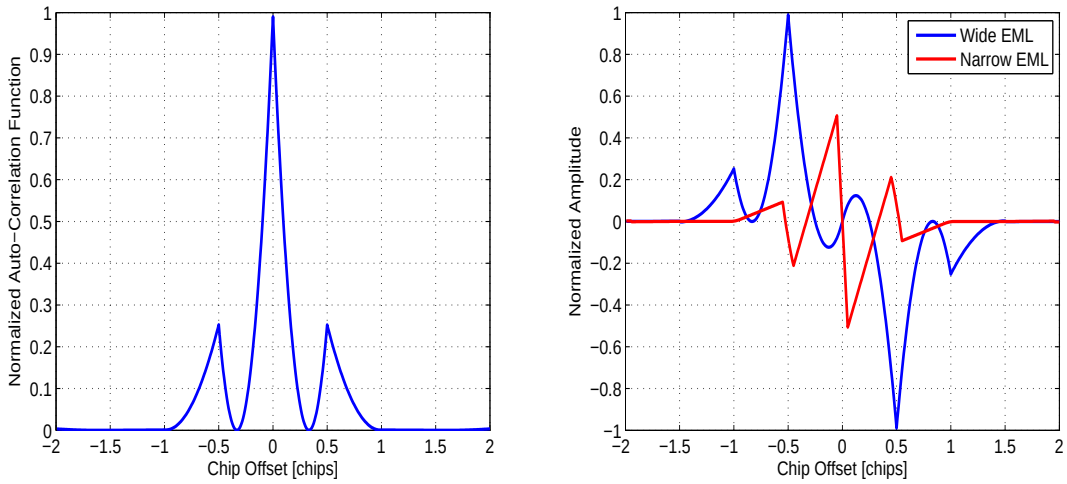

Figure 6.1: ACF of SinBOC(1,1) modulated signal (left plot) and the corresponding discriminator functions for wide ($\Delta_{WEML} = 1$ chip) and narrow ($\Delta_{NEML} = 0.05$ chips) correlators (right plot) in single path static channel model

$$D_{NEML}(\tau) = \left| R(\tau + \frac{\Delta_{NEML}}{2}) \right|^2 - \left| R(\tau - \frac{\Delta_{NEML}}{2}) \right|^2, \tag{6.2}$$

where $R(\tau)$ is the ACF of the received signal and auto-generated replica code, and Δ_{NEML} is the early-late chip spacing for narrow EML.

Figure 6.1 represents the resulting discriminator function, D_{NEML} (i.e., S-curve) for narrow EML computed from ACF of the received signal and auto-generated replica code in the receiver of a GNSS system. In here, the channel delay is signalled by a zero crossing from above.

The advantages of narrow chip spacing are the reduction of tracking errors in the presence of both noise and multipath. Noise reduction is achieved with narrow spacing because the noise components of the early and late signals are correlated and tend to cancel, provided that early and late processing are simultaneous. And, multipath effects are reduced because the DLL discriminator is less distorted by the delayed multipath signal. On the contrary, the primary disadvantage of narrow spacing is that a wider precorrelation bandwidth is required, coupled with higher sample rates and higher digital signal processing rates. [84]

In what follows, the term 'wide EML' is used instead of wide correlator and the term 'narrow EML' is used instead of narrow correlator. The code multipath performance for wide EML and narrow EML will be presented in section 8.4.

6.3 High Resolution Correlator

The term double delta ($\Delta\Delta$) correlator is a general expression for special code discriminators which are formed by more than 3 correlators in the tracking loop. The general tracking concept is described in detail in [88, 89], where this type of correlator is called High Resolution Correlator (HRC). In HRC, 5 correlators are formed: two early, one in-prompt and two late (with respect to the sampling point of interest), denoted in what follows via E_1, E_2, P, L_1 and L_2, respectively. Then a discriminator function is formed of the type:

$$D_{HRC} = a(E_1 - L_1) - b(E_2 - L_2), \tag{6.3}$$

where a and b are two variables of the model.

According to [88], the values for a and b are 1 and 0.5, respectively. The general concept of HRC is illustrated in Figure 6.2, where the spacing between E_1 and L_1 is referred to as Δ_{HRC} and the spacing between E_2 and L_2 is referred to as $2\Delta_{HRC}$ and $R(\tau)$ is the ACF of the received signal and the locally generated reference signal [88]. There are some

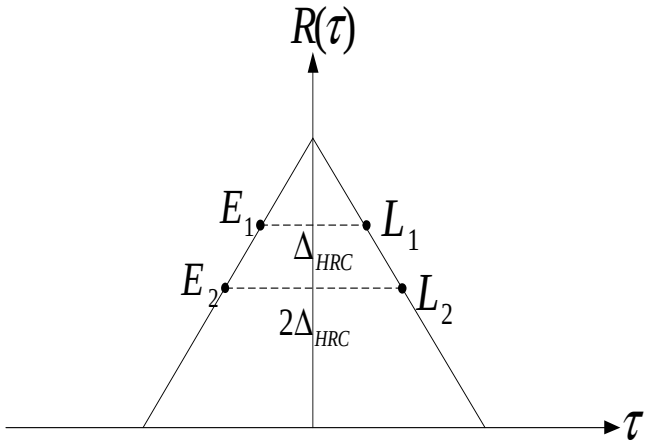

Figure 6.2: General concept of HRC [89]

other variants of $\Delta\Delta$ correlators: namely, the strobe correlator of Ashtech [90] (with a=2, b=1), and Pulse Aperture Correlator (PAC) of NovAtel [91] (with a=2, b=1). However, the differences between them are minor, therefore it is enough to focus on HRC.

6.4 Multiple Gate Delay Correlator

The conventional EML discriminators for BOC modulated signals mentioned earlier have multiple zero crossings, which can produce false lock positions. These false lock positions

produce a bias in the estimated ToA. In order to cope with this problem, a new unambiguous tracking technique known as Multiple Gated Delay (MGD) was introduced in [92, 93, 94]. The tracking structure of MGD is quite similar with $\Delta\Delta$ correlators. Like $\Delta\Delta$ correlators, MGD has a number of early and late gates and the appropriately chosen weighting factors used to combine them in the discriminator. According to [94], MGD has the discriminator function of the type:

$$D_{MGD} = \frac{\sum_{n=1}^{N} a_n[E_n - L_n]}{\sum_{n=1}^{N} a_n[E_n + L_n]}, \tag{6.4}$$

where the coefficients a_n are used to shape the response of the discriminator, E_n and L_n are the n-th early and the n-th late gates of the tracking loop, respectively. In this thesis work, the variables are chosen as: $N = 4$, $a_1 = 1$, $a_2 = -1/4$, $a_3 = 1/2$ and $a_4 = -3/4$. The variables are chosen based on extensive analysis of MGD in terms of semi-analytical MEEs as presented in section 8.4.

MGD is very sensitive to the parameters (i.e., weighting factors and number of correlators) chosen in the discriminator function and still is the subject of an ongoing study, specially, in case of multipath distortion.

6.5 Multipath Estimating Delay Lock Loop

Multipath Estimating Delay Lock Loop (MEDLL) is mainly designed to reduce both code and carrier multipath errors by estimating the parameters (i.e., amplitudes, delays, phases) of LOS plus multipath signals [95, 96]. The MEDLL of NovAtel uses several correlators (e.g., 6 to 10) per channel in order to determine accurately the shape of the multipath-corrupted correlation function. Then, a reference correlation function is used in a software module in order to determine the best combination of LOS and NLOS components (i.e., amplitudes, delays, phases and number of multipaths). An important aspect of the MEDLL is an accurate reference correlation function which could be constructed by averaging measured correlation functions over a significant amount of total averaging time [96].

In the presence of multipath propagation, the received signal at the input of a DSSS receiver can be written as: [85]

$$r(t) = \sum_{m=0}^{M-1} A_m p(t - \tau_m) cos(wt + \theta_m) + \eta(t), \tag{6.5}$$

where -

M = number of signals
t = time
$p(t)$ = the spread spectrum code
$\eta(t)$ = white Gaussian noise
A_m = component signal amplitude
τ_m = component signal delay
θ_m = component signal phase

The MEDLL approach involves the decomposition of correlation function into its direct and multipath components. The MEDLL estimates the amplitude (A_m), delay (τ_m) and phase (θ_m) of each multipath component using maximum likelihood criteria. Each estimated multipath correlation function is in its turn subtracted from the measured correlation function. After the completion of this process, only the estimate of the direct path correlation function is left. Finally, a standard EML DLL is applied to the direct path component and an optimal estimate of the code tracking error is obtained. [85, 97]

Performance evaluation of narrow EML, wide EML and MEDLL in terms of multipath mitigation capability is presented in [85]. The MEDLL shows better performance than narrow and wide EML DLLs, but it does not completely eliminate all multipath errors. Especially multipath signals with small relative delays are difficult to eliminate. However, the advantage of MEDLL is that it reduces the influence of multipath signals significantly on the code and carrier estimates of the LOS signal by estimating both LOS and multipath parameters mentioned above.

6.6 Differential Order 2 Scheme

Slope Differential (SD) is the recent multipath mitigation scheme based on the slope difference of the prompt correlator output between the received signal and the locally generated reference signal. This technique is first proposed in [98]. The architecture of the SD scheme is presented in Figure 6.3. The advantage of SD scheme is that it does not require a high speed digital signal processing for the narrow early-late spacing since it employs only the prompt correlator unlike EML, HRC or MGD [98].

The baseband equivalent received signal $c_r(t)$ of the Galileo system under the multipath environment can be expressed as: [98]

$$c_r(t) = \sum_{m=0}^{M-1} A_m c(t - \tau_m), \tag{6.6}$$

where $c(t)$ is the positioning code in Galileo systems; A_0 and τ_0 represent the amplitude and delay of the LOS signal, respectively; $A_{m,m\neq 0}$ and $\tau_{m,m\neq 0}$ mean the amplitude and delay of the m-th multipath signal, respectively; and M is the number of signals.

The SD scheme can estimate the path delay of the LOS signal as follows: [98]

$$\hat{\tau_0} = arg \ \max_{l} \ \frac{d^2}{dl^2} \left[\int_0^{NT_c} c_r(t)c(t-l)dt \right], \tag{6.7}$$

where $\hat{\tau_0}$ is the estimated delay of the LOS signal, N is the code period, and T_c is the chip duration of the positioning code.

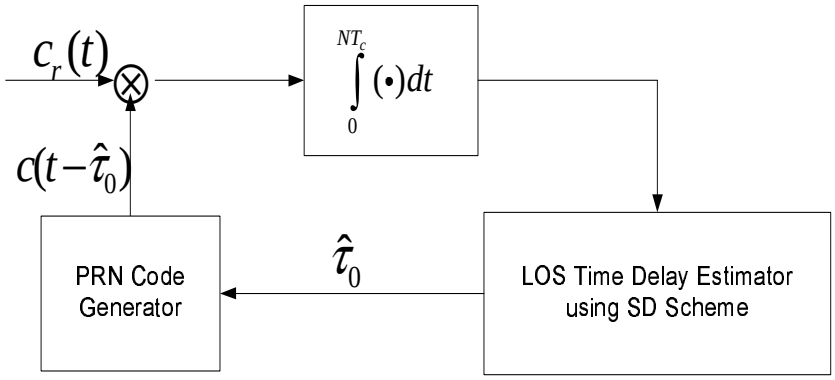

Figure 6.3: The architecture of Slope Differential scheme [98]

Differential Order 2 (Diff2) scheme is slightly modified version of SD scheme. In SD, it is assumed that the amplitude of the LOS signal is always larger than the amplitude of the multipath signal which is not always true in real life situations. Diff2 considers a threshold based on the estimated noise level N_{Thresh} plus some weight factor W_D multiplied by the maximum l_{max} of the 2^{nd} order differential obtained from equation 6.7. The weight factor W_D is chosen in such a way that it can compensate the side lobes of ACF of SinBOC(1,1) modulated signal. Unlike SD, where only l_{max} is used directly in order to estimate the delay of the LOS path, Diff2 uses an adaptive threshold $Diff2_{Thresh}$ which can be obtained using the following equation:

$$Diff2_{Thresh} = l_{max} \ W_D + N_{Thresh} \tag{6.8}$$

Because of using this adaptive threshold, Diff2 could estimate the first path delay even in multipath profiles where the first path power is less than or equal to the consecutive path powers.

Figure 6.4 represents a plot for 2 path Rayleigh fading channel model with fixed multipath separation of 0.5 chips. Here, the path powers are [0 -3] dB and CNR is considerably high, i.e., 100 dB-Hz. The computed Diff2 threshold and the noise threshold are shown in the figure. According to figure 6.4, it can be noticed that the first Diff2 peak corresponds to

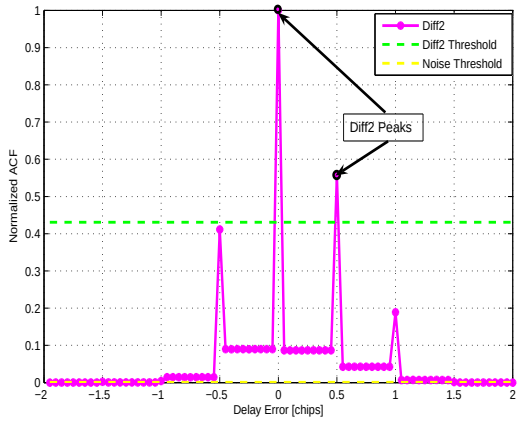

Figure 6.4: Delay estimation of the LOS path using Diff2 scheme

the delay of the LOS path whereas the second Diff2 peak is the delay of the second path which is 0.5 chips away from the first path.

6.7 Matched Filter

The Matched Filter (MF) concept is extensively studied in [79, 99, 100]. As explained earlier, MF is based on a threshold computation which is determined according to the channel condition provided by the feed-forward loop. At first, the noise level is estimated and then a linear threshold is computed based on the noise variance plus some weight factor obtained from feed-forward loop. The choice of weight factor is crucial since it has to be chosen such that the side lobe peaks of the ACF of the received signal and locally generated PRN code can be compensated. Therefore, the first peak of MF which is above the linear threshold corresponds to the estimated delay of the LOS path.

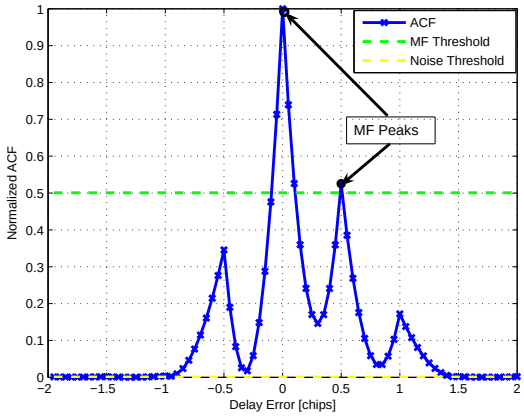

Figure 6.5: Delay estimation of the LOS path using MF

Figure 6.5 represents the plot for the same path profile as it was described in the previous section. Here also, the computed MF threshold and the noise threshold are shown in the figure. According to Figure 6.5, it is visible that the first peak which is above the MF threshold is the estimated delay of the LOS path.

Chapter 7

Proposed Algorithm: Peak Tracking

The aim of the development of the new novel PT algorithm is to find such an algorithm that fully utilizes the advantages of both feed-forward and feed-back techniques and improves the fine delay estimation. PT utilizes the adaptive threshold obtained from the feed-forward loop in order to determine the competitive delays, i.e., the delays which are competing as being the actual delay (i.e., the delay of the first arriving path). The adaptive threshold is based on the estimated noise variance of the ACF of the received signal and the locally generated reference signal. At the same time, PT explores the advantage of feed-back loop by calculating weight factors based on the previous estimation in order to take decision about the actual delay. However, the utilization of feed-back loop is always a challenge since there is a chance to propagate the delay error to subsequent estimations. Therefore, the delay error should remain in tolerable range (for example, less than or equal to half of the width of main lobe) so that the advantage from feed-back loop could be properly utilized.

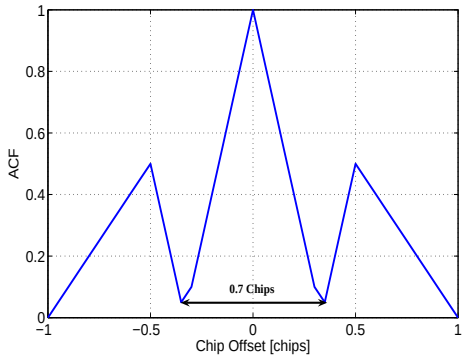

Figure 7.1: Ideal ACF of SinBOC(1,1) modulated signal

In case of SinBOC(1,1) modulated signal, the width of main lobe of an ideal ACF of

the locally generated reference signal is about 0.7 chips as shown in Figure 7.1. PT algorithm is applied to SinBOC(1,1) modulated signal and, therefore, assumes a maximum allowable delay error as less than or equal to half of the width of the main lobe (i.e., $0.7/2 = 0.35$ chips). The simulation results regarding maximum tolerable delay error for different algorithms will be presented in section 8.2.

7.1 Description of PT Algorithm

The terminologies used in the algorithm are defined in this section. The procedure of the algorithm is explained with some illustrative figures in section 7.2.

7.1.1 ACF Peak

In this context, the term ACF peak is defined as any local maximum point greater than a specific threshold (i.e., ACF_{Thresh}, explained in section 7.1.4) in the ACF distribution of the received signal and the locally generated reference signal. The ACF peaks (ACF_{Peak}) are actually the normalized amplitudes of local maximum points in the ACF domain which can be obtained using the following equation:

$$ACF_{Peak} = \forall x\{(x \in ACF) \wedge (x >= ACF_{Thresh})\}, \tag{7.1}$$

where ACF is the autocorrelation function of the received signal and the locally generated reference signal, ACF_{Thresh} is the ACF Threshold which is defined in equation 7.3, and $\hat{L}_{ACF}$ is the cardinality of the set ACF_{Peak}.

7.1.2 Diff2 Peak

Diff2 peak is defined as any local maximum point greater than a specific threshold (i.e., $Diff2_{Thresh}$, explained in section 7.1.5) in the 2^{nd} order differential distribution, obtained by 2^{nd} order differentiation of the ACF of the received signal and the locally generated reference signal. The Diff2 peaks ($Diff2_{Peak}$) are actually the normalized amplitudes of local maximum points in the 2^{nd} order differential domain which can be obtained using the following equation:

$$Diff2_{Peak} = \forall x\{(x \in Diff2) \wedge (x >= Diff2_{Thresh})\}, \tag{7.2}$$

where $Diff2$ is the 2^{nd} order differentiation of the ACF of the received signal and the locally generated reference signal, $Diff2_{Thresh}$ is the Diff2 Threshold which is defined in equation 7.5, and $\hat{L}_{Diff2}$ is the cardinality of the set $Diff2_{Peak}$.

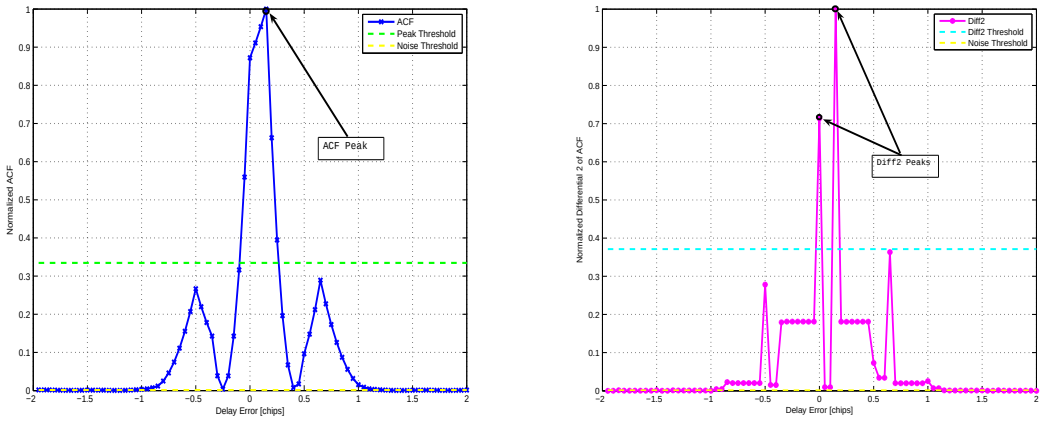

Figure 7.2: ACF Peak (left), Diff2 Peaks (right) of PT algorithm

In Figure 7.2, ACF peak and Diff2 peaks are marked according to the definition described earlier. Figure 7.2 represents a plot for 2 path Rayleigh fading channel model with fixed path separation of 0.15 chips. Here, the path powers are [-2 0] dB and CNR is considerably high, i.e., 100 dB-Hz, in order to emphasize the multipath channel effect. According to Figure 7.2, it is visible that the first Diff2 peak corresponds to the delay of the LOS path whereas the first and only ACF peak corresponds to the delay of the second path which is 0.15 chips away from the first path. The experience from the simulation emphasizes the fact that Diff2 could distinguish very closely spaced paths whereas there might not be ACF peaks to distinguish very closely spaced paths. On the contrary, Diff2 is very sensitive to noise specially in low CNR, and therefore, Diff2 does not perform well in low CNR scenarios.

7.1.3 Noise Threshold

Noise Threshold (N_{Thresh}) is obtained by estimating the noise level of the ACF of the received signal and the locally generated reference signal. The noise level is estimated by taking the mean of out-of-peak values of the ACF. The out-of-peak values are those local maximum points which fall outside the rectangular window as shown in Figure 7.3. The rectangular window should be such that it can enclose the side lobe peaks of the ACF, and hence, the width of the rectangular window should not be less than 2 chips. In this example case, the width of the rectangular window was 2.4 chips.

7.1.4 ACF Threshold

ACF Threshold (ACF_{Thresh}) is basically computed from the estimated noise threshold N_{Thresh} obtained from feed-forward loop and a weight factor W_{ACF} using the following

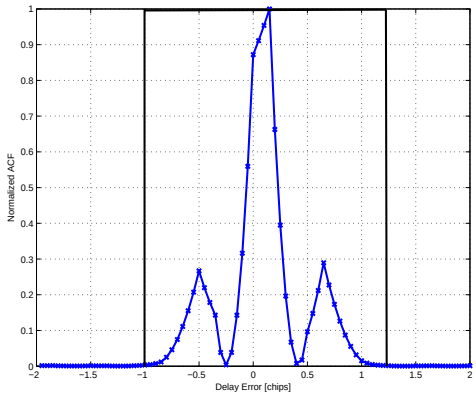

Figure 7.3: Estimation of noise threshold

equation:

$$ACF_{Thresh} = W_{ACF} + N_{Thresh}, \tag{7.3}$$

where ACF_{Peak} and N_{Thresh} were defined in sections 7.1.1 and 7.1.3, respectively; and W_{ACF} is defined as follows:

$$0.3 <= W_{ACF} <= 0.35 \tag{7.4}$$

W_{ACF} was chosen very carefully taking into consideration the side lobes of ACF of SinBOC(1,1) modulated signal. Figure 7.4 represents an ideal non-coherent ACF of SinBOC(1,1) modulated signal where the side lobe peaks correspond to the value 0.25, approximately. Therefore, W_{ACF} could be chosen according to equation 7.4 in order to avoid side lobe peaks being considered as the competitive peaks. Definition of competitive peaks is presented in section 7.1.6.

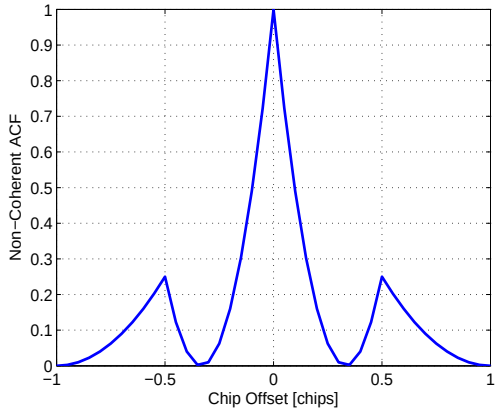

Figure 7.4: Ideal non-coherent ACF (i.e., squared ACF) of SinBOC(1,1) modulated signal

7.1.5 Diff2 Threshold

Diff2 Threshold ($Diff2_{Thresh}$) is computed from the estimated noise threshold N_{Thresh} obtained from feed-forward loop and a weight factor W_D using the following equation:

$$Diff2_{Thresh} = max\{Diff2_{Peak}\}W_D + N_{Thresh}, \tag{7.5}$$

where $Diff2_{Peak}$ and N_{Thresh} were defined in sections 7.1.2 and 7.1.3, respectively; and W_D is defined as follows:

$$0.37 <= W_D <= 0.5 \tag{7.6}$$

The 2^{nd} order differentiation of ACF is very sensitive to noise which emphasized the fact that the weight factor W_D should be chosen higher than the weight factor W_{ACF} chosen for ACF_{Thresh}. That is why, the weight factor W_D is slightly greater than W_{ACF}. The details of Diff2 scheme has already been explained in section 6.6.

7.1.6 Competitive Peak

Competitive Peak (C_{Peak}) can be obtained using the following equation:

$$C_{Peak} = \{(ACF_{Peak}) \cup (Diff2_{Peak})\} \tag{7.7}$$

$$T_{ACF}(\tau_i) = ACF(\tau_i);\ i = 1, \ldots, \hat{L} \tag{7.8}$$

$$T_{Diff2}(\tau_i) = Diff2(\tau_i);\ i = 1, \ldots, \hat{L}\ , \tag{7.9}$$

where ACF and $Diff2$ were defined in sections 7.1.1 and 7.1.2, respectively; and, $\hat{L}$ is the cardinality of the set C_{Peak}, denoted as follows:

$$|C_{Peak}| = \hat{L} \tag{7.10}$$

Since, for GNSS applications, the point of interest is to find the delay of the first arriving path (i.e., the LOS path), therefore, it would be enough to consider first 5 competitive peaks at most. Hence, PT assumes that:

$$\max(\hat{L}) = 5 \tag{7.11}$$

Figure 7.5 shows the competitive peaks for the same path profile as in Figure 7.2 and 7.3. The competitive peaks are obtained using equation 7.7. As it can be seen from Figure 7.5, for this particular example, there are in total 2 competitive peaks which compete to be considered as being the actual delay of the LOS path. In this example, the first competitive peak corresponds to the delay of the first arriving path whereas the second competitive peak corresponds to the delay of the second arriving path which is 0.15 chips apart from the first path.

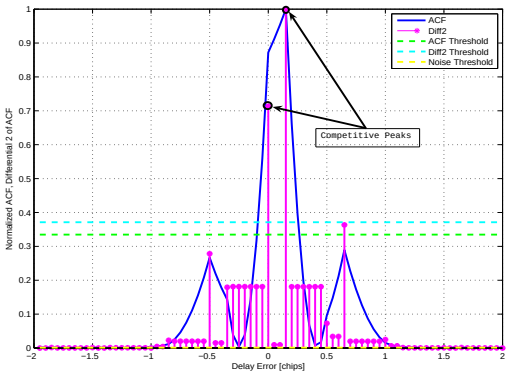

Figure 7.5: Competitive peaks of PT algorithm

7.2 Procedure of PT Algorithm

The general architecture of PT algorithm is shown in Figure 7.6. In what follows, the step by step procedure of PT algorithm is presented.

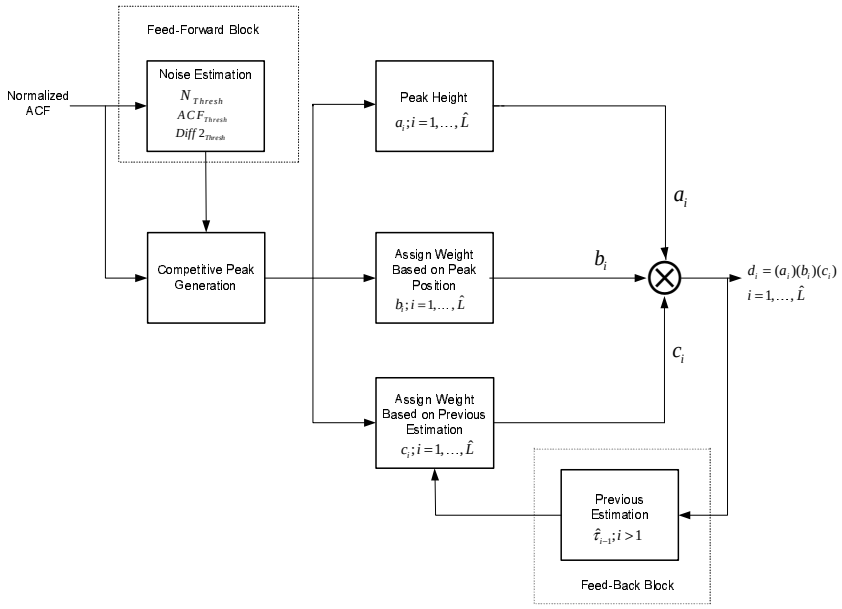

Figure 7.6: The general architecture of PT algorithm

7.2.1 Step 1: Noise Estimation

N_{Thresh} is estimated according to section 7.1.3, which is then used to determine ACF_{Thresh} and $Diff2_{Thresh}$ with the help of equations 7.3 and 7.5. These thresholds are then provided as input to the next step.

7.2.2 Step 2: Competitive Peak Generation

Step 2(a): Look for ACF peak(s) in ACF domain using equation 7.1.
Step 2(b): Look for Diff2 peak(s) in Diff2 domain using equation 7.1.
Step 2(c): Find competitive peak(s) using equation 7.7.

The competitive peak(s) obtained from step 2 are then fed into steps 3(a), 3(b) and 3(c) in order to assign some weights in each sub-step for each particular competitive peak.

7.2.3 Step 3(a): Weight Based on Peak Height

Assign weight(s) $(a_i);\ i = 1, \ldots, \hat{L}$ based on the competitive peak height(s) using the following equation:

$$a_i = [T_{ACF}(\tau_i) + T_{Diff2}(\tau_i)]/2;\ i = 1, \ldots, \hat{L}\ , \tag{7.12}$$

where T_{ACF} and T_{Diff2} are defined is section 7.1.6.

7.2.4 Step 3(b): Weight Based on Peak Position

Assign weight(s) $b_i;\ i = 1, \ldots, \hat{L}$ based on peak positions in ACF distribution: the first peak is more probable than the second one; the second one is more probable than the third one and so on. This is based on the assumption that typical multipath channel has decreasing power-delay profile. In the simulation, the following weights were used based on peak positions:

$$[b_1\ b_2\ b_3\ b_4\ b_5] = [10\ 8\ 6.2\ 5.5\ 5] \tag{7.13}$$

where $b_i,\ i = 1, \ldots, \hat{L}$ denotes the weight factor for i^{th} peak; i.e., b_1 is the weight for 1^{st} peak, b_2 is the weight for 2^{nd} peak, and, so on. It is very logical to assign higher weights for the first few competitive peaks as compared to later peaks since the target is to find the delay of the first path. However, the weights are optimized through trial and error method based on extensive analysis of the Monte Carlo simulation results.

7.2.5 Step 3(c): Weight Based on Previous Estimation

Assign weight(s) $c_i;\ i = 1, \ldots, \hat{L}$ based on the feed-back from the previous estimation: the closer the competitive peak is from the previous estimation, the higher the weight would be for that particular competitive peak. Figure 7.7 illustrates the mapping of weight(s) (c_i) based on the previous estimation. For example, for a delay difference of 0.1 chips from the previous estimation, the weight factor (c_i) would be 10, and for a delay difference of 0.2 chips, the weight factor (c_i) would be 9 and so on.

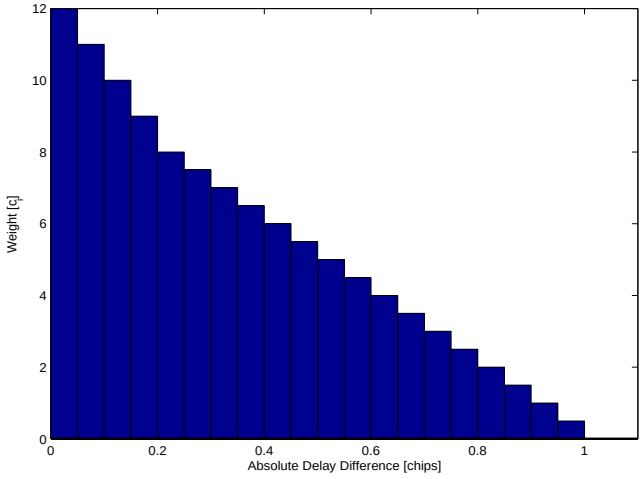

Figure 7.7: Mapping of weights $(c_i, i = 1, \ldots, \hat{L})$ based on previous estimation

7.2.6 Step 4: Compute Decision Variable

Decision variable, $d_i; i = 1, \ldots, \hat{L}$ is computed according to the following equation:

$$d_i = a_i b_i c_i;\ i = 1, \ldots, \hat{L} \tag{7.14}$$

7.2.7 Step 5: Find Estimated Delay of the LOS Path

Estimated delay of the LOS path can be obtained using the following equation:

$$\hat{\tau}_{LOS} = arg \max_{i=1:\hat{L}}(d_i) \tag{7.15}$$

Table 7.1 summarizes the weights assigned in the example path profile shown in Figure 7.5. In this example case, there are two competitive peaks meaning that we need to assign weights only for those two peaks. In assigning weights for $c_i; i = 1, \ldots, \hat{L}$, PT

Table 7.1: Assignment of weights for Figure 7.5

1^{st} Competitive Peak	a_1	b_1	c_1	d_1
	0.8	10	12	96
2^{nd} Competitive Peak	a_2	b_2	c_2	d_2
	1	8	10	80

assumes that there is no initial error present from the previous estimation. In step 4, the algorithm simply computes the decision variable $d_i; i = 1, \ldots, \hat{L}$ using equation 7.14 for each competitive peak. And, finally, in step 5, PT algorithm selects the peak which has the maximum value for decision variable d_i. In our case, it is d_1. Therefore, in this example case, the first competitive peak corresponds to the delay of the LOS path.

Chapter 8

Performance Analysis

In this chapter, the performance of the discussed code tracking algorithms is compared in terms of RMSE, MTLL, delay error variance and semi-analytical MEEs. The simulation results are provided in section 8.2 for different multipath profiles in Rayleigh fading channel model. The estimated delay variance obtained from the simulations are then compared with the theoretical CRB [101, 102] which is presented in section 8.3. Finally, the performance of feed-back code tracking algorithms and the proposed PT algorithm is analyzed in terms of MEEs.

8.1 Common Parameters Used in Simulations

All the simulations have been carried out in multipath Rayleigh fading channel model for SinBOC(1,1) modulated Galileo OS signal. The common parameters used in all the simulations are mentioned in Table 8.1. Unless otherwise stated, the value for the corresponding parameter is unchanged. The channel parameters which are varying from

Table 8.1: Common parameters with their values for all the simulations

Parameter	**Symbol**	**Value**	**Unit**
Spreading Factor	S_F	20	chips
Oversampling Factor	N_S	16	-
Early-late Chip Spacing	Δ	0.1	chips
Channel Delay Increment	Δ_{inc}	0.05	chips
Coherent Integration Length	N_C	20	ms
Non-coherent Integration Length	N_{NC}	6	blocks

simulation to simulation are specified while describing the result of that particular simulation. As specified in Table 8.1, the meaning of channel delay increment is that a fixed channel delay was introduced to the randomly varying channel in each subsequent delay

estimation (i.e., in each subsequent Monte Carlo iteration). The amount of fixed channel delay increment was 0.05 chips in each subsequent delay estimation. Therefore, the channel was always varying linearly by 0.05 chips after each delay estimation by which we mean 'channel delay increment'. Here, it is to mention that the oversampling factor N_S is the number of samples per BOC interval. According to Table 8.1, the spreading factor S_F used in the simulations was set to 20 chips instead of 1024 or 4092 chips in order to avoid high execution time required to run each simulation. However, the low value of S_F should not affect the simulation results since the code tracking operation was performed on narrowband signal after despreading. The only effect of a lower S_F would be worse code crosscorrelation properties, thus slightly worse results than those with a higher S_F. However, because of this, we do not expect a change in the relative performance of various algorithms.

8.2 Simulation Results

Extensive simulations have been carried out targeted to achieve the following results:

- RMSE vs. CNR
- MTLL vs. CNR
- RMSE vs. First Path Power
- RMSE vs. Multipath Spacing
- RMSE vs. Initial Delay Error

The performance of the code tracking algorithms is analyzed in this section for different path profiles and the most representative results have been included. In what follows, RMSE / MTLL vs. CNR / First Path Power / Multipath Spacing / Initial Delay Error results are shown for two illustrative cases: *i. without any channel delay increment*, and *ii. with non-zero constant channel delay increment* in order to figure out the sensitivity of different feed-back DLLs (i.e., code tracking algorithms) with the constant variation of the channel.

8.2.1 RMSE / MTLL vs. CNR

Two main path profiles are considered here, namely, 2 path profile with equal path power (i.e., path power: [0 0] dB) spaced randomly between 0 and 0.5 chips; and 3 path profile with path power 0, -1 and -2 dB, respectively, where each path is spaced randomly from the successive path by a maximum of 0.5 chips.

2 Path Profile

Figure 8.1 represents **RMSE vs. CNR** curves without any channel delay increment (left plot) and with non-zero constant channel delay increment (right plot) for the following path profile: 2 path Rayleigh fading channel model with path power [0 0] dB where two paths are spaced randomly between 0 and 0.5 chips. The simulation assumed no initial delay error. The simulation was carried out from CNR 20 dB-Hz to 45 dB-Hz. For each particular CNR, the total number of Monte Carlo iterations was set to 10000 ($200 * 50 = 10000$).

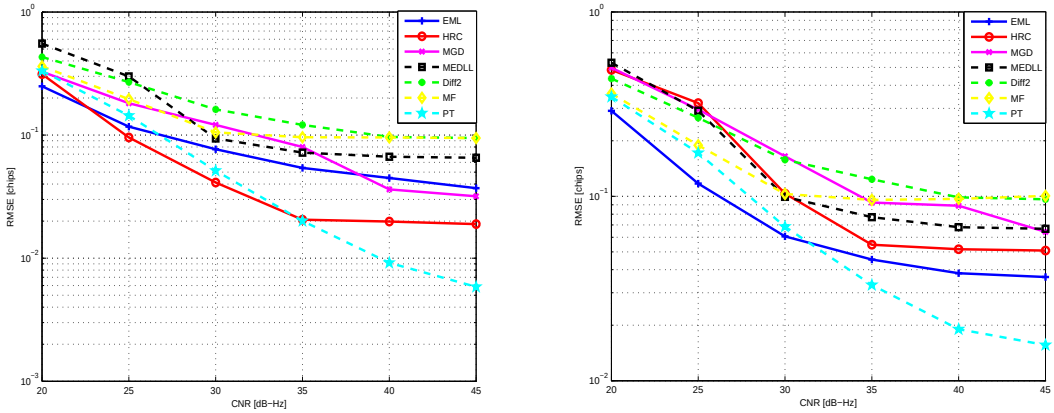

Figure 8.1: RMSE vs. CNR plots without any channel delay increment (left plot) and with non-zero constant channel delay increment (right plot) for 2 path Rayleigh fading channel model

According to Figure 8.1, the feed-back algorithms show better performance as compared to the feed-forward algorithms in both the cases (i.e., with non-zero constant linear channel variation and with no channel variation). In the above path profile, PT shows the most promising performance among all the algorithms from CNR 35 dB-Hz to onwards. HRC is more sensitive to channel variations than EML and hence, performs worse in linear channel delay variation as compared to EML. This is mainly because of the fact that HRC has more false lock points than EML which makes it more challenging to lock at the correct zero crossing of S-curve.

Figure 8.2 represents the corresponding **MTLL vs. CNR** curves for the preceding path profile. The feed-back algorithms show better performance as compared to the feed-forward algorithms in terms of MTLL. This is obvious because the feed-back algorithms utilize the previous delay estimation provided from the feed-back loop and there was no initial delay error assumed in the simulations for both the cases. The maximum value for MTLL was 6000 ms ($50 * N_C * N_{NC} = 6000$ ms) or 6 seconds.

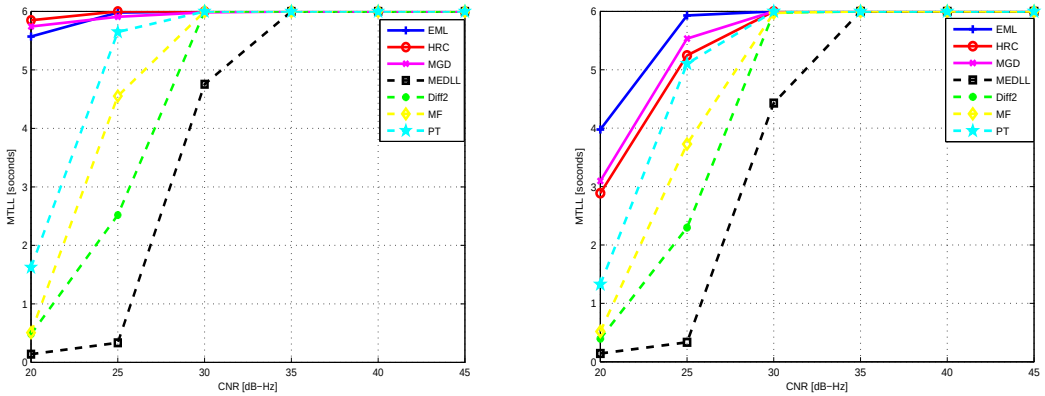

Figure 8.2: MTLL vs. CNR plots without any channel delay increment (left plot) and with non-zero constant channel delay increment (right plot) for 2 path Rayleigh fading channel model

According to Figures 8.1 and 8.2, it can be noticed that the algorithms based on many correlators (i.e., more than 3 correlators) like HRC and MGD were affected much by the linear channel delay increment as compared to conventional EML.

3 Path Profile

Figure 8.3 represents **RMSE vs. CNR** curves without any channel delay increment (left plot) and with non-zero constant channel delay increment (right plot) for the following path profile: 3 path Rayleigh fading channel model with path power [0 -1 -2] dB where three paths are separated randomly with a maximum of 0.5 chips separation from the successive path. The simulation assumed no initial delay error. The simulation was carried out from CNR 20 dB-Hz to 45 dB-Hz. For each particular CNR, the total number of Monte Carlo iterations was set to 10000.

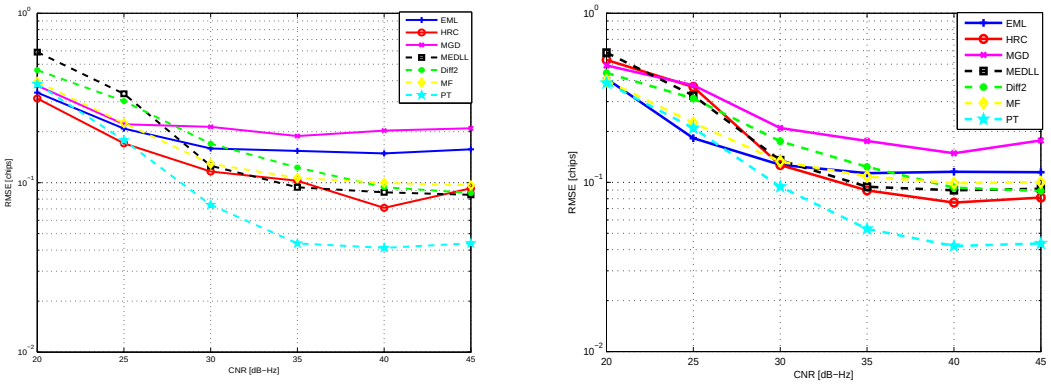

Figure 8.3: RMSE vs. CNR plots without any channel delay increment (left plot) and with non-zero constant channel delay increment (right plot) for 3 path Rayleigh fading channel model

According to Figure 8.3, it is worthwhile to mention that the feed-back algorithms do not show better performance in 3 path closely spaced profile in good CNR scenarios (i.e., from 30 dB-Hz to onwards) as compared to the feed-forward algorithms in terms of RMSE. However, PT distinctively shows the best performance in both the cases from CNR 30 dB-Hz to onwards. And, HRC and MEDLL are two other competitive algorithms showing good performance in the above path profile.

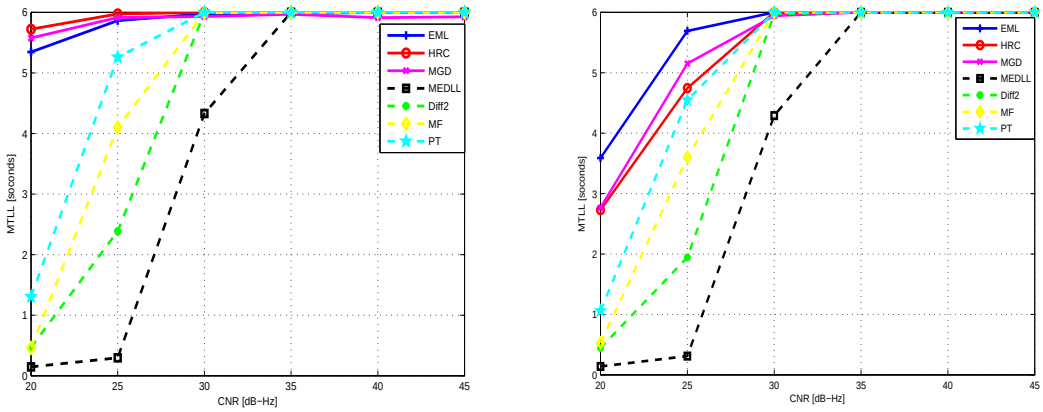

Figure 8.4: MTLL vs. CNR plots without any channel delay increment (left plot) and with non-zero constant channel delay increment (right plot) for 3 path Rayleigh fading channel model

Figure 8.4 represents the corresponding **MTLL vs. CNR** curves for the preceding path profile. As expected, the feed-back algorithms show better performance as compared to the feed-forward algorithms in terms of MTLL. The maximum value for MTLL was 6 seconds. Here also, the performance degradation of the feed-back algorithms in terms of MTLL can be noticed with linear channel delay increment as explained earlier.

8.2.2 RMSE vs. First Path Power

Figure 8.5 represents **RMSE vs. First Path Power** curves without any channel delay increment (left plot) and with non-zero constant channel delay increment (right plot) for the following path profile: 2 path Rayleigh fading channel model with path power [A 0] dB where two paths are spaced randomly with a maximum of 0.5 chips separation and A denotes the average first path power in dB. The average first path power A was varying from -3 dB to $+3$ dB whereas the average second path power was always 0 dB. The simulation assumed no initial delay error. The simulation was carried out for CNR 40 dB-Hz. For each particular 2 path profile with varying average first path power, the total number of Monte Carlo iterations was set to 10000.

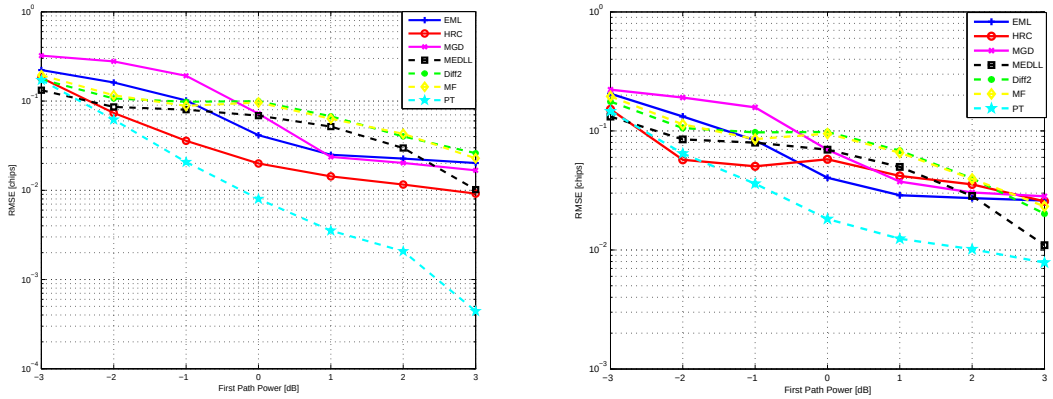

Figure 8.5: RMSE vs. First Path Power plots without any channel delay increment (left plot) and with non-zero constant channel delay increment (right plot) for 2 path Rayleigh fading channel model where first path varies from −3 dB to +3 dB and second path is always 0 dB

According to Figure 8.5, it can be noticed that the performance of PT is very promising as compared to other code tracking algorithms. Though HRC provides competitive result in constant channel profile, it does not seem to be very promising in case of path profiles with linear channel delay increment. In real life situation, it is quite natural to have some drift in the channel delay due to the random nature of propagation channel.

8.2.3 RMSE vs. Multipath Spacing

Figure 8.6 represents **RMSE vs. Multipath Spacing** curves without any channel delay increment (left plot) and with non-zero constant channel delay increment (right plot) for the following path profile: 2 path Rayleigh fading channel model with path power [0 0] dB

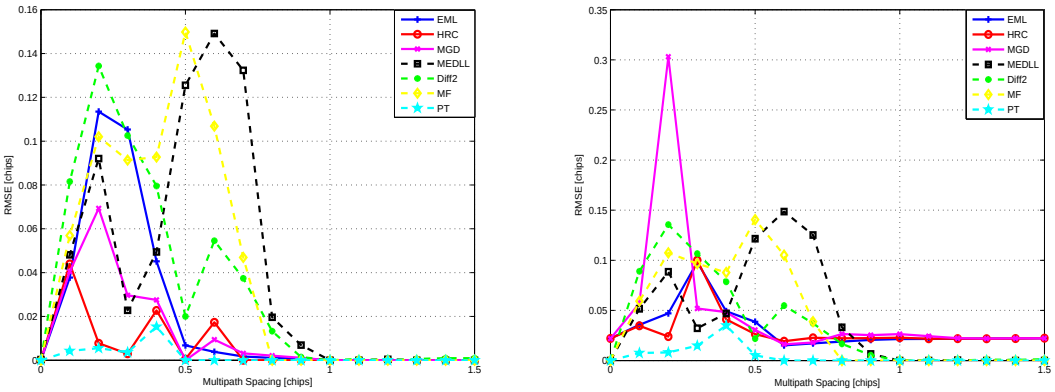

Figure 8.6: RMSE vs. Multipath Spacing plots without any channel delay increment (left plot) and with non-zero constant channel delay increment (right plot) for 2 path Rayleigh fading channel model with multipath separation from 0 to 1.5 chips

where two paths are spaced from each other by a constant chip spacing varying from 0 to 1.5 chips. The simulation assumed no initial delay error. The simulation was carried out for CNR 40 dB-Hz. For each particular 2 path profile with fixed multipath separation, the total number of Monte Carlo iterations was set to 10000.

As presented in the left plot of Figure 8.6, the feed-back algorithms show much better performance than the feed-forward algorithms in constant 2 path channel profile. But, it is not the case with constant variation of channel delay as depicted in the right plot of Figure 8.6. In this case, the feed-back algorithms never converge to zero RMSE even in distant multipath separation. This is mainly because of the fact that the feed-back algorithms are solely dependent on the previous estimation and if there is any variation in the channel delay (which is true in our case), it will affect the estimation of current delay. However, PT provides the most promising result in both the cases since PT not only considers the information from the feed-back loop but also utilizes the statistical properties of ACF of the received signal and locally generated reference signal in order to take decision about the correct delay estimate.

8.2.4 RMSE vs. Initial Delay Error

Figure 8.7 represents **RMSE vs. Initial Delay Error** curves without any channel delay increment (left plot) and with non-zero constant channel delay increment (right plot) for the following path profile: 2 path Rayleigh fading channel model with path power [0 0] dB where two paths are spaced randomly between 0 and 0.5 chips. Initial delay error was varying from 0 to 0.35 chips. The simulation was carried out for CNR 40 dB-Hz. For each particular 2 path profile with varying initial delay error, the total number of Monte Carlo iterations was set to 10000.

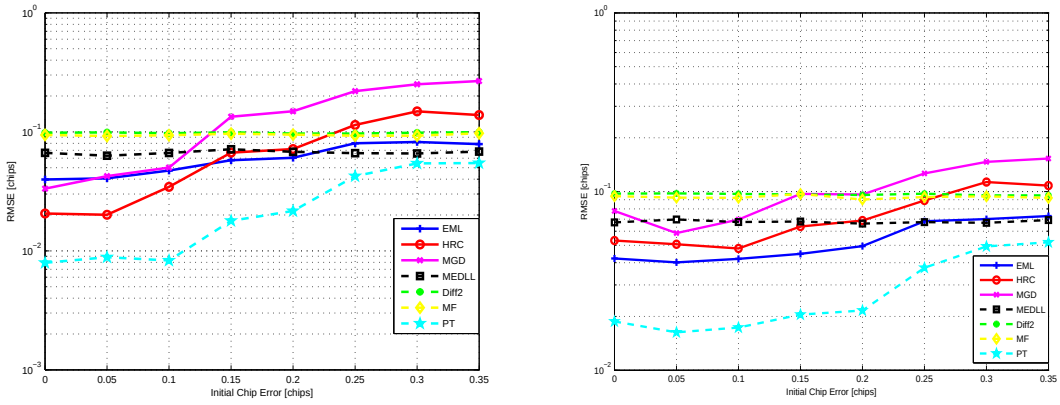

Figure 8.7: RMSE vs. Initial Delay Error plots without any channel delay increment (left plot) and with non-zero constant channel delay increment (right plot) for 2 path Rayleigh fading channel model with varying initial delay error from 0 to 0.35 chips

According to Figure 8.7, it can be easily understood that initial delay error has no affect on the feed-forward algorithms (i.e., MEDLL, MF, Diff2) as expected because the current delay estimate does not depend on the previous estimates, whereas the feed-back algorithms are affected more due to initial delay error. The advantage of the feed-back loop could be realized only when the delay error to subsequent iterations can be kept in tolerable range. Different algorithms have different tolerance range depending on the channel parameters of multipath profiles. However, the novel PT algorithm has a tolerable range of approximately half of the width of the main lobe (i.e., 0.35 chips) of the ACF of SinBOC(1,1) modulated signal as shown in Figure 8.7.

8.3 Comparison with CRB

A measure of the performance of any timing estimator is the lower bound of its variance, given by the well-known CRB [101, 102]. A Modified Cramer-Rao Lower Bound (MCRLB) for multipath time-delay estimation for DS-CDMA systems is proposed in [101]. According to [101], in MCRLB, the lower variance bound of each estimated path delay is determined using the theoretical results. Here, the theoretical results obtained from MCRLB are compared with the simulation results discussed in the previous section for different path profiles.

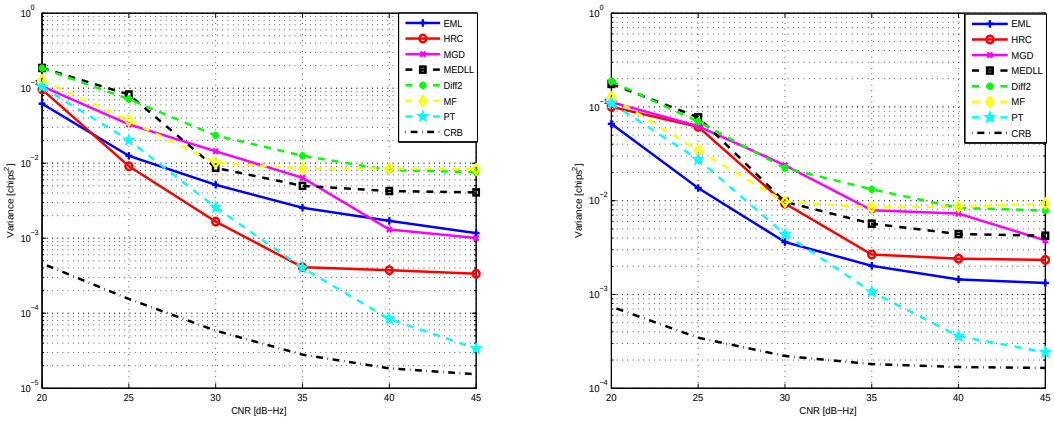

Figure 8.8: Variance vs. CNR plots without any channel delay increment (left plot) and with non-zero constant channel delay increment (right plot) for 2 path Rayleigh fading channel model

Figure 8.8 represents **Variance vs. CNR** curves without any channel delay increment (left plot) and with non-zero constant channel delay increment (right plot) for 2 path profile discussed in section 8.2. The variance of the delay of the first path tends to approach the theoretical MCRLB bound when the CNR is high enough. However, the variance of

the estimated delay of the first path obtained from PT algorithm clearly approaches the theoretical MCRLB bound with the increase in CNR.

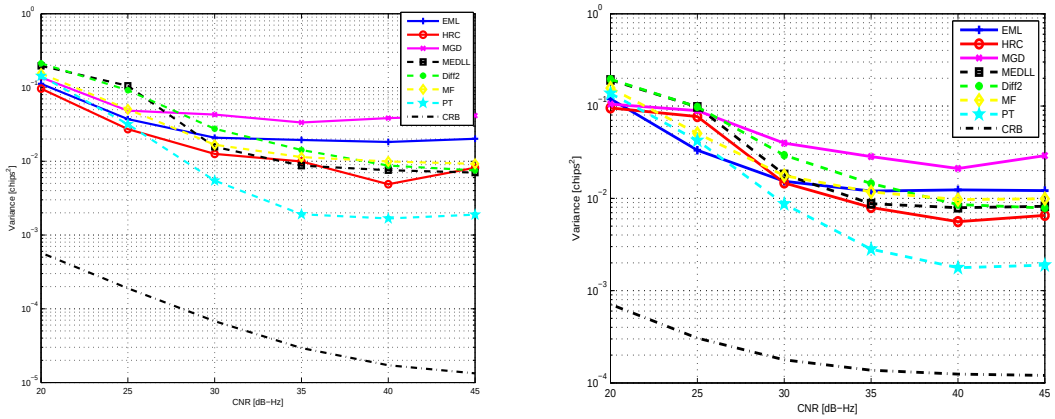

Figure 8.9: Variance vs. CNR plots without any channel delay increment (left plot) and with non-zero constant channel delay increment (right plot) for 3 path Rayleigh fading channel model

Another illustrative example for 3 path profile discussed in section 8.2 is presented in Figure 8.9. The gap between the simulation results and the theoretical MCRLB bound is clearly visible in Figure 8.9 which indicates the fact that still there is scope to improve the performance of the discussed code tracking algorithms.

8.4 Semi-Analytical MEEs Computation

The signal received over a fading multipath channel (after Doppler removal) can be written as: [76, 103]

$$r(t) = \sum_{m=1}^{M} \alpha_m s_{SinBOC}(t - \tau_m) + \eta(t), \tag{8.1}$$

where M is the number of channel paths, α_m is the channel complex coefficient of the m-th path, τ_m is the channel delay of the m-th path, $s_{SinBOC}(t)$ is the SinBOC(1,1) modulated code sequence and $\eta(t)$ is the additive white Gaussian noise of the channel.

At the output of the receiver correlator, the following can be obtained: [76, 103]

$$R(\tau) = E\left(\int r(t) s_{SinBOC}(t - \tau) dt\right), \tag{8.2}$$

where τ is the tentative delay estimate of the first channel path τ_1 and $E(\cdot)$ is the expectation operator.

Typically, theoretical and semi-analytical MEEs are computed in the absence of noise, and when only two paths are present (the direct LOS component and an interfering path at an arbitrary distance τ_Δ). Thus, for coherent DLL, equation 8.2 becomes:

$$R(\tau) = \sum_{m=1}^{2} \alpha_m R_{SinBOC}(\tau - \tau_1 - (m-1)\tau_\Delta), \tag{8.3}$$

with $R_{SinBOC}(\tau)$ being the autocorrelation function of a SinBOC(1,1) modulated code sequence. The discriminator functions (i.e., S-curves) for non-coherent WEML, NEML, HRC and MGD are defined in equations 6.1-6.4.

The computed semi-analytical MEEs for 2 path with the second path being 3 dB less than the first path are presented in Figure 8.10. In the figure, the delay error (in chips)

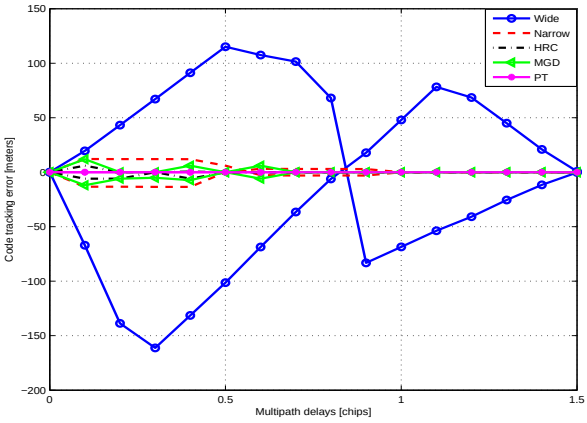

Figure 8.10: Multipath error envelopes for non-coherent wide EML, narrow EML, HRC and PT code tracking algorithms

is converted in meters (one chip corresponds to 293.2551 meters for a chip rate of 1.023 Mcps). According to Figure 8.10, it is clear that PT and HRC are the two most competitive code tracking algorithms in terms of semi-analytical MEEs which provide minimal delay error as compared to other algorithms. In the simulation, we used oversampling factor $N_S = 60$, BOC modulation order $N_{BOC} = 2$, and therefore, a delay error less than 2.4438 meters (i.e., $\frac{1}{N_S * N_{BOC}} * 293.2551 = 2.4438$) can not be detectable with our current model.

Chapter 9

Conclusions and Future Work

This chapter presents the conclusions obtained from the research results of this thesis and draws recommendations for future work.

9.1 Conclusions

The purpose of this thesis was to analyze some representative code tracking algorithms for SinBOC(1,1) modulated Galileo OS signal. The analysis was performed in order to measure the performance of these algorithms in different multipath fading channel environments. The algorithms analyzed in the context of this thesis include both feed-back and feed-forward structures since both of these techniques attract significant research interests for several years. All these algorithms were tested from pure tracking point-of-view for SinBOC(1,1) modulated Galileo OS signal and their performance were measured with various well-known criteria such as RMSE, MTLL, MEEs and so on.

It was shown in Chapter 7 that the main problem faced by SinBOC(1,1) modulated signal is the presence of high autocorrelation side peaks within the range of ± 1 chip. This could result in a false acquisition or biased tracking, either of which could be extremely crucial since they would strongly degrade the final positioning solution if not corrected. An innovative code tracking algorithm dedicated to SinBOC(1,1) modulated signal, namely PT was introduced in the thesis for this purpose. PT can be considered as a combination of both feed-back and feed-forward structures since it not only utilizes the information from the feed-forward loop but also takes into consideration the previous estimation fed from the feed-back loop. Therefore, the advantages inherent in feed-back and feed-forward structures are also present in PT with some additional complexity required to estimate the noise threshold in the feed-forward loop. By doing so, PT was shown to provide a very good tracking accuracy as presented in Chapter 8.

Feed-back code tracking algorithms consider the previous estimation fed from the feed-back loop in order to decide the present delay estimation. Therefore, these algorithms are solely based on feed-back information, and hence, are greatly affected by initial delay error as it is quite expected to have a code delay error by a certain amount from the code acquisition stage. In order to utilize the best from feed-back code tracking structure, it has to be ensured that the code delay error should be kept within certain limit. However, a code delay error greater than 0.35 chips would inevitably result in a loss of lock or in ambiguous tracking in case of implementing feed-back structure. The reason is obvious from the fact that an ideal ACF of SinBOC(1,1) modulated signal has side peaks at about ± 0.5 chips away from the main peak which was described in Chapter 7.

The novel PT algorithm showed very promising results in various multipath profiles, specially in good CNRs (i.e., from 35 dB-Hz to onwards). Moreover, the delay error variance for PT algorithm obtained from the simulation was approaching to theoretical CRB with increasing CNR in 2 path Rayleigh fading channel model, and, achieved a result which is near to maximum attainable from theory.

9.2 Future Work

The results shown using the traditional and PT code tracking algorithms were built on the assumption of SinBOC(1,1) modulation. However, this work can be extended as analyzing the performance of these algorithms for other representative BOC modulation such as CosBOC(15,2.5), CosBOC(10,5) and so on.

The analyzed feed-forward algorithms were optimized as much as possible through out the research work. However, it is still possible to modify and improve Diff2 and MF algorithms since these two algorithms are quite new and require a lot of attention for future research, specially in more complex channel profiles, such as Nakagami fading or nonlinear variation of the channel delays.

The focus of this thesis was limited to Rayleigh fading channel model, and therefore, the future work can be focused on Nakagami-m fading channel model which was proposed as the best fit for satellite-to-indoor radio wave propagation in [57, 58].

Finally, although the simulation tools used in this thesis were designed to meet the actual conditions, it would be beneficial to test the most significant code tracking algorithms on real data.

Bibliography

[1] E. D. Kaplan. *Understanding GPS - Principles and Applications*. Artech House Publishers, Boston, 1996.

[2] K. Kovach and K. V. Dyke. GPS in Ten Years. In *Proceedings of the US Institute of Navigation GPS Conference*, pages 1251–1259, Kansas City, MS, USA, September 1997.

[3] European Commission. GALILEO Involving Europe in a New Generation of Satellite Navigation Services. COM 54 Final.

[4] GPS World. GNSS on Stage. Available via <http://www.gpsworld.com>.

[5] G. W. Hein, J. Godet, J. L. Issler, J. C. Martin, P. Erhard, R. L. Rodriguez, and T. Pratt. Status of Galileo Frequency and Signal Design. In *CDROM Proceedings of ION GPS*, September 2002.

[6] J. W. Betz. Binary Offset Carrier Modulations for Radio Navigation. *Navigation: Journal of the Institute of Navigation*, 48(4):227–246, 2002.

[7] J. W. Betz and D. B. Goldstein. Candidate Design for an Additional Civil Signal in GPS Spectral Bands. In *Proceedings of the US Institute of Navigation NTM Conference*, pages 622–631, San Diego, CA, USA, January 2002.

[8] O. Julien, C. Macabiau, G. Lachapelle, M.E. Cannon, and C. Mongrédien. A New Unambiguous BOC(n,n) Signal Tracking Technique. In *CD-ROM Proceedings of the European Navigation Conference GNSS*, Rotterdam, The Netherlands, May 2004.

[9] P. Fine and W. Wilson. Tracking Algorithm for GPS Offset Carrier Signals. In *Proceedings of the US Institute of Navigation NTM Conference*, pages 25–27, San Diego, CA, USA, January 1999.

[10] V. S. Lin, P. A. Dafesh, A. Wu, and C. R. Cahn. Study of the Impact of the False Lock Points on Subcarrier Modulated Ranging Signals and Recommended Mitigation Approaches. In *Proceedings of the US Institute of Navigation AM Conference*, pages 156–165, Albuquerque, NM, USA, June 2003.

[11] P. Ward. A Design Technique to Remove the Correlation Ambiguity in Binary Offset Carrier (BOC) Spread Spectrum Signals (Revised Version). In *Proceedings of the US Institute of Navigation NTM Conference*, pages 886–896, San Diego, CA, USA, January 2004.

[12] J. J. Caffery Jr. and G. L. Stüber. Overview of Radiolocation in CDMA Cellular System. *IEEE Communications Magazine*, 36(4):38–45, April 1998.

[13] A. Lakhzouri. *Channel estimation and Mobile Phone Positioning in CDMA Based Wireless Communications Systems*. PhD thesis, Tampere University of Technology, June 2005.

[14] R.L. Peterson, R.E. Ziemer, and D. E. Borth. *Introduction to Spread Spectrum Communications*. Prentice Hall, 1995.

[15] J. J. Spilker. Fundamentals of Signal Tracking Theory in Global Positioning System: Theory and Applications Volume I. *Progress in Astronautics and Aeronautics, volume 164, AIAA*, pages 245–328, 1997.

[16] Capt. B. C. Barker, J. W. Betz, J. E. Clark, J. T. Correia, J. T. Gillis, S. Lazar, Lt. K. A. Rehborn, and J. R. Straton. Overview of the GPS M Code Signal. In *Proceedings of Intitute of Navigation National Tech. Meeting: Navigating into the New Millennium*, pages 542–549, January 2000.

[17] Galileo Joint Undertaking - The European Programme for Global Navigation Services. Available via <http://www.galileoju.com>.

[18] G. W. Hein, M. Irsigler, J. A. A. Rodriguez, and T. Pany. Performance of Galileo L1 Signal Candidates. In *Proceedings of The European Navigation Conference (ENC-GNSS)*, 2004.

[19] COSPAS-SARSAT web site. International Satellite System for Search and Rescue. Available via <http://www.cospas-sarsat.org>. referred May 12, 2006.

[20] European Commission: Directorate General for Energy and Transport. GALILEO: An Imperative for Europe. Available via <http://europa.eu.int>.

[21] GPS-Galileo Working Group A (WG A). Recommendations on L1 OS/L1C Optimization. WGA Recommendation March 22, 2006.

[22] G. W. Hein, J. A. A. Rodriguez, S. Wallner, A. R. Pratt, J. Owen, and J. L. Issler. MBOC: The New Optimized Spreading Modulation Recommended for Galileo L1 OS and GPS L1C. Available via <http://forschung.unibw-muenchen.de>.

[23] J. W. Betz. The Offset Carrier Modulation for GPS modernization. In *Proceedings of ION National Technical Meeting (ION-NTM '99)*, pages 639–648, January 1999.

[24] O. Julien. *Design of Galileo L1F Receiver Tracking Loops*. PhD thesis, University of Calgary, July 2005.

[25] E. S. Lohan, A. Lakhzouri, and M. Renfors. Binary Offset Carrier modulation techniques with applications in satellite navigation systems. *Wiley Journal of Wireless Communications and Mobile Computing*, in print 2006.

[26] E. S. Lohan, A. Lakhzouri, and M. Renfors. Spectral Shaping of Galileo Signals in the Presence of Frequency Offsets and Multipath Channels. In *CDROM Proceedings of IST Mobile & Wireless Communications Summit*, Dresden, Germany, June 2005.

[27] R. L. Pickholtz, D. L. Schilling, and L. B. Milstein. Theory of Spread Spectrum Communications - A Tutorial. *IEEE Transactions on Communications*, COM-30(5):855–884, May 1982.

[28] T. Ojanperä and R. Prasad. *Wideband CDMA for Third Generation Mobile Communications*. Artech House Publishers, 1998.

[29] S. Glisic and B. Vucetic. *Spread Spectrum CDMA Systems for Wireless Communications*. Artech House Publishers, 1997.

[30] UMTS World. Available via: <http://www.umtsworld.com>. referred July 10, 2006.

[31] R. A. Scholtz M. K. Simon, J. K. Omura and B. K. Levitt. *Spread Spectrum Communications, volume 1, Electrical Engineering Communications and Signal Processing*. Computer science press, Inc., Rockvill, Maryland 20850, 1 edition, 1985.

[32] R. Skaug and J. F. Hjelmstad. *Spread Spectrum in Communication, IEE Telecommunications series*. Peter Peregrinus Ltd., London, UK, 1985.

[33] J. K. Holmes. *Coherent Spread Spectrum Systems*. Wiley, New York, 1982.

[34] R. C. Dixon. *Spread Spectrum Systems*. Wiley, New York, second edition, 1984.

[35] N. Yee, J. P. Linnartz, and G. Fettweis. Multi-Carrier CDMA in Indoor Wireless Radio Networks. In *Proceedings of PIMRC'93*, pages 109–113, Yokohama, Japan, 1993.

[36] V. K. Garg, K. Smolik, and J. E. Wilkes. *Applications of CDMA in Wireless/Personal Communications*. Prentice Hall, 1997.

[37] A. J. Viterbi. *CDMA: Principles of Spread Spectrum Communication*. Addison-Wesley, 1995.

[38] G. Gao, J. Spilker, D. Akos, S. Lo, A. Chen, and P. Enge. Code Generators Used by the Galileo L1 Signal. GPS lab, April 25 2006. Stanford University.

[39] T. S. Rappaport. *Wireless Communications: Principles and Practice*. Prentice Hall, 1996.

[40] J. Proakis. *Digital Communications*. McGraw-Hill, New York, USA, 1995.

[41] E. Pajala. Code-Frequency Acquisition Algorithms for BOC Modulated CDMA Signals with Applications in Galileo and GPS Systems. Master's thesis, Tampere University of Technology, August 2005.

[42] S. Haykin and M. Moher. *Modern Wireless Communications*. Prentice Hall, 2005.

[43] H. Bertoni. *Radio Propagation for Modern Wireless Systems*. Prentice Hall, 2000.

[44] S. Saunders. *Antennas and Propagation for Wireless Communication Systems*. Wiley, New York, 2000.

[45] R. Vaughan and J. B. Anderson. *Channels, Propagation and Antennas for Mobile Communications*. IEE, 2003.

[46] J. D. Parsons. *The Mobile Radio Propagation Channel*. Pentech Press Ltd, 1992.

[47] R. N. Pupala. Introduction to Wireless Electromagnetic Channels & Large Scale Fading. Lecture notes for Wireless Communication Technologies course offered by Prof. N. Mandayan, Spring 2005. Department of Electrical Engineering, Rutgers University.

[48] A. Paulraj, R. Nabar, and D. Gore. *Introduction to Space-Time Wireless Communication Systems*. Cambridge University Press, 2003.

[49] F. Belloni. Fading Models. S-72.333 Postgraduate Course in Radio Communications, Autumn 2004. S-88 Signal Processing Laboratory, Helsinki University of Technology.

[50] A. Richter, R.S. Thomae, and T. Taga. Directional Measurement and Analysis of Propagation Path Variation in a Street Micro-Cell Scenario. In *Proceedings of* 57^{th} *IEEE Vehicular Technology Conference (VTC 2003-Spring)*, Jeju, Korea, April 2003.

[51] A. F. Molisch. *Wideband Wireless Digital Communications*. Prentice Hall, 2000.

[52] S. Benedetto, E. Biglieri, and R. Daffara. Performance of Multilevel Baseband Digital Systems in a Nonlinear Environment. *IEEE Transactions on Communications*, 24(10):1166–1175, October 1976.

[53] L. Greenstein. A Multipath Fading Channel Model for Terrestrial Digital Radio Systems. *IEEE Transactions on Communications*, 26(8):1247–1250, August 1978.

[54] W. Kumwilaisak and C. C. J. Kuo. Adaptive Variable Length Markov Chain for Non-stationary Fading Channel Modeling. In *Proceedings of IEEE GLOBE-COM*, volume 3, pages 2046–2050, 2002.

[55] F. Zhu, Z. Wu, and C. R. Nassar. Generalized Fading Channel Model with Application to UWB. In *Proceedings of IEEE Conference on Ultra Wideband Systems and Technologies*, volume 1, pages 13–17, 2002.

[56] M. K. Simon and M. S. Alouini. *Digital Communication over Fading Channels*. John Wiley & Sons, 2000.

[57] A. Lakhzouri, E. S. Lohan, I. Saastamoinen, and M. Renfors. Measurement and Characterization of Satellite-to-Indoor Radio Wave Propagation Channel. In *Proceedings of The European Navigation Conference (ENC-GNSS '05)*, Münich, Germany, July 2005.

[58] A. Lakhzouri, E. S. Lohan, I. Saastamoinen, and M. Renfors. Interference and Indoor Channel Propagation Modeling Based on GPS Satellite Signal Measurements. In *In Proceedings of ION-GPS*, pages 896–901, September 2005.

[59] M. Nakagami. The m-distribution - A General Formula of Intensity Distribution of Rapid Fading. In *W. C. Hoffman: Statistical Methods of Radio Wave Propagation*, pages 3–36, Oxford, England, 1960.

[60] Wikipedia Article on Rayleigh Fading. <http://en.wikipedia.org>. referred August 6, 2006.

[61] A. Lakhzouri, E. S. Lohan, R. Hamila, and M. Renfors. EKF Channel Estimation for LOS Detection in WCDMA Mobile Positioning. *EURASIP Journal of Applied Signal Processing*, 13:1268–1278, December 2003.

[62] W. R. Braun and U. Dersch. A physical mobile radio channel model. *IEEE Trans. Veh. Technol.*, 40:472–482, May 1991.

[63] A. Polydoros and C. L. Weber. A Unified Approach to Serial Search Spread-Spectrum Code Acquisition - Parts I and II: A Matched-Filter Receiver. *IEEE Transactions on Communications*, 32(5):542–560, May 1984.

[64] M. Katz. *Code Acquisition in Advanced CDMA Networks.* PhD thesis, University of Oulu, Oulu, Finland, 2002.

[65] F. V. Diggelen and C. Abraham. Indoor GPS Technology. Presented at CTIA Wireless agenda, Dallas, Texas, May 2001.

[66] W. Zhuang. Noncoherent Hybrid Parallel PN Code Acquisition for CDMA Mobile Communications. In *International Conference on Wireless Communications*, Calgary, Canada, July 1995.

[67] E. A. Sourour and S. C. Gupta. Direct-Sequence Spread-Spectrum Parallel Acquisition in a Fading Mobile Channel. *IEEE Transactions on Communications*, 38(7):992–998, July 1990.

[68] E. S. Lohan, A. Lakhzouri, and M. Renfors. Selection of the Multiple-Dwell Hybrid-Search Strategy for the Acquisition of Galileo Signals in Fading Channels. In *Personal and Indoor Mobile Radio Communications (PIMRC)*, volume 4, pages 2352–2356, Barcelona, Spain, September 2004.

[69] C. Baum and V. Veeravalli. Hybrid Acquisition Schemes for Direct Sequence CDMA Systems. In *Proceedings of ICC 94, SUPERCOMM/ICC '94, Conference Record, Serving Humanity Through Communications. IEEE International Conference*, volume 3, pages 1433–1437, May 1994.

[70] B. J. Kang, H. R. Park, and Y. Han. Hybrid acquisition in DS/CDMA forward link. In *Proceedings of Vehicular Technology Conference, 1997 IEEE 47th*, volume 3, pages 2123–2127, May 1997.

[71] S. M. Deshpande. Study of Interference Effects on GPS Signal Acquisition. Master's thesis, Department of Geomatics Engineering, University of Calgary, Calgary, Alberta, July 2004.

[72] J. Jung. Implementation of Correlation Power Peak Ratio Based Signal Detection Method. In *Proceedings of ION GNSS 17th International Technical Meeting of the Satellite Division*, Long Beach, CA, September 2004.

[73] J.Pang, F. V. Graas, J. Starzyk, and Z. Zhu. Fast Direct GPS P-code Acquisition. *GPS Solutions*, 7(3):168–175, 2003.

[74] S. M. Kay. *Fundamentals of Statistical Signal Processing, Vol 2.: Detection Theory.* Prentice Hall, 1993.

[75] E. S. Lohan. *Multipath delay estimators for fading channels with applications in CDMA receivers and mobile positioning*. PhD thesis, Tampere University of Technology, October 2003.

[76] E. S. Lohan, R. Hamila, A. Lakhzouri, and M. Renfors. Highly Efficient Techniques for Mitigating the Effects of Multipath Propagation in DS-CDMA Delay Estimation. *IEEE Transactions on Wireless Communications*, 4(1):149–162, January 2005.

[77] R. De Gaudenzi, M. Luise, and R. Viola. A Digital Chip Timing Recovery Loop for Band-Limited Direct-Sequence Spread Spectrum Signals. *IEEE Transactions on Communications*, 41(11):1760–1769, November 1993.

[78] M. Latva-aho. *Advanced Receivers for Wideband CDMA systems*. PhD thesis, University of Oulu, October 1998.

[79] E. S. Lohan, A. Lakhzouri, and M. Renfors. Feedforward Delay Estimators in Adverse Multipath Propagation for Galileo and Modernized GPS Signals. EURASIP Journal on Applied Signal Processing, in print 2006.

[80] G. Fock, J. Baltersee, P. Schulz-Rittich, and H. Meyr. Channel Tracking for RAKE Receivers in Closely Spaced Multipath Environments. *IEEE Journal on Selected Areas in Communications*, 19(12):2420–2431, 2001.

[81] P. S. Rittich, G. Fock, J. Baltersee, and H. Meyr. Low Complexity Adaptive Code Tracking with Improved Multipath Resolution for DS-CDMA Communications over Fading Channels. In *Proceedings of IEEE ISSSTA*, volume 1, pages 30–34, September 2000.

[82] H. Boujemaa and M. Siala. Enhanced Coherent Delay Tracking for Direct Sequence Spread Spectrum Systems. In *Proceedings of IEEE ISSTA*, volume 1, pages 274–277, September 2000.

[83] M. Laxton. Analysis and Simulation of a New Code Tracking Loop for GPS Multipath Mitigation. Master's thesis, Airforce Institute of Technology, Dayton, Ohio, USA, 1996.

[84] A. J. V. Dierendonck, P. C. Fenton, and T. Ford. Theory and Performance of Narrow Correlator Spacing in a GPS Receiver. *Journal of The Institute of Navigation*, 39(3), June 1992.

[85] B. R. Townsend, R. D. J. V. Nee, P.C. Fenton, and K. J. V. Dierendonck. Performance Evaluation of the Multipath Estimating Delay Lock Loop. In *Insitute of Navigation National Technical Meeting*, Anaheim, CA, USA, January 1995.

[86] P. Fenton. Pseudorandom noise ranging receiver which compensates for multipath distortion by making use of multiple correlator time delay spacing. NovAtel Patent, US 5 414 729, May 1995.

[87] P. Fenton and A. J. V. Dierendonck. Pseudorandom noise ranging receiver which compensates for multipath distortion by dynamically adjusting the time delay spacing between early and late correlators. NovAtel Patent, US 5 495 499, Feb 1996.

[88] G. A. McGraw and M. S. Braasch. GNSS Multipath Mitigation Using Gated and High Resolution Correlator Concepts. In *Proceedings of the National Technical Meeting of the Satellite Division of the Insitute of Navigation*, San Diego, USA, January 1999.

[89] M. Irsigler and B. Eissfeller. Comparison of Multipath Mitigation Techniques with Consideration of Future Signal Structures. In *CDROM Proceedings of ION-GNSS*, Portland, Oregon, September 2003.

[90] L. Garin and J. M. Rousseau. Enhanced Strobe Correlator Multipath Rejection for Code and Carrier. In *Proceedings of ION-GPS*, pages 559–568, 1997.

[91] P. Fenton, B. Smith, and J. Jones. Theory and Performance of Pulse Aperture Correlator. NovAtel Technical Paper. Available via <http://www.novatel.com>.

[92] R. Fante. Unambiguous Tracker for GPS Binary-Offset Carrier Signals. In *Proceedings of the 2003 ION National Technical Meeting*, Albuquerque, New Mexico, 2003.

[93] R. Fante. Unambiguous First-Order Tracking Loop M-Code. MITRE Technical Report, July 2004. MTR 94B0000040.

[94] R. Fante. Code Tracking Performance for Novel Unambiguous M-code Time Discriminators. In *Proceedings of the 2005 ION National Technical Meeting*, San Diego, CA, January 2005.

[95] R. D. J. V. Nee. The Multipath Estimating Delay Lock Loop. In *IEEE Second International Symposium on Spread Spectrum Techniques and Applications*, pages 39–42, Yokohama, Japan, November 29 - Dec 02 1992.

[96] R. D. J. V. Nee, J. Sierveld, P.C. Fenton, and B.R. Townsend. The Multipath Estimating Delay Lock Loop: Approaching Theoretical Accuracy Limits. In *IEEE Position Location and Navigation Symposium*, volume 1, pages 246–251, 1994.

[97] B. R. Townsend, P.C. Fenton, K. J. V. Dierendonck, and R. D. J. V. Nee. L1 Carrier Phase Multipath Error Reduction Using MEDLL Technology. In *Proceedings of 8th International Technical Meeting of the Satellite Division of the Insitute of Navigation*, Palm Springs, CA, USA, September 1995.

[98] C. Lee, S. Yoo, S. Yoon, and S. Y. Kim. A Novel Multipath Mitigation Scheme Based on Slope Differential of Correlator Output for Galileo Systems. In *Proceedings of 8th International Conference on Advanced Communication Technology*, February 20-22 2006.

[99] J. Joutsensalo. Algorithms for Delay Estimation and Tracking in CDMA. In *Proceedings of IEEE ICC*, volume 1, pages 366–370, 1997.

[100] J. Iinatti. *Matched Filter Code Acquisition Employing a Median Filter in Direct Sequence Spread-Spectrums with Jamming.* PhD thesis, University of Oulu, 1997.

[101] E. S. Lohan, R. Hamila, and M. Renfors. Cramer Rao Bound for Multipath Time Delays in a DS-CDMA System. In *Proceedings of WPMC'01*, volume 2, pages 1043–1046, September 2001.

[102] C. Botteron, A. H. Madsen, and M. Fattouche. Cramer-Rao bound for location estimation of a mobile in asynchronous DS-CDMA systems. In *Proceedings of ICASSP'01*, volume 4, pages 2221–2224, Salt Lake City, UT, USA, 2001.

[103] J. Selva. *Efficient Multipath Mitigation in Navigation Systems.* PhD thesis, Department of Signal Theory and Communications, Universitat Politecnica de Catalunya, 2004.